

# Synthesis and characterization of NASICON based materials

A Dissertation for

**PHY-651:Dissertation**

**Credits: 16**

Submitted in partial fulfilment of Masters degree in Physics

by

**RIYA SINGH**

Seat Number: 22PO430040

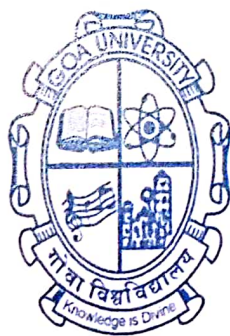
ABC ID: 730533569964

PRN: 201802297

Under the Supervision of

**BHOLANATH PAHARI**

School of Physical and Applied Sciences



**GOA UNIVERSITY**  
**MAY 2024**



Examined by:

*Ry*

Seal of the School

### DECLARATION BY STUDENT

I hereby declare that the data presented in this Dissertation report entitled, "Synthesis and characterization of NASICON based materials" is based on the results of investigations carried out by me in the Master of Physics in Science at the School of Physical and Applied Sciences at the Goa University under the Supervision of Dr Bholanath Pahari and the same has not been submitted elsewhere for the award of a degree or diploma by me. Further, I understand that Goa University or its authorities will be not be responsible for the correctness of observations / experimental or other findings given the dissertation.'

I hereby authorize the University authorities to upload this dissertation on the dissertation repository or anywhere else as the UGC regulations demand and make it available to any one as needed.



Riya Singh

22P0430040

Date: 09/05/2024

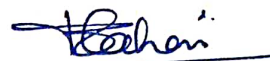
Place: Goa University

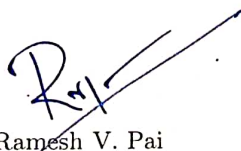
## COMPLETION CERTIFICATE

This is to certify that the dissertation report "Synthesis and characterization of NASICON based materials" is a bonafide work carried out by Ms. Riya Rajesh Singh under my supervision in partial fulfilment of the requirements for the award of the degree of M.Sc in Physics at the School of Physical and Applied Sciences, Goa University.

Supervisor: Dr. Bholanath Pahari

Sign:

  
09/05/2024 .



Dean: Prof. Ramesh V. Pai

School of Physical and Applied Sciences

Sign:

Date: 09/05/2024

Place: Goa University



School Stamp

## Acknowledgements

I would like to express my deep gratitude and respect to my guide, **Dr. Bholanath Pahari** for his keen interest and valuable guidance during the course of work. I also thank him for his great patience and useful suggestions. I am also thankful to **Dr. Bhargav Alvani** and **Ms. Pallavi Pandhari Gaude** for their useful suggestions to overcome the errors occurred in latex while writing the project.

I would like to thank **Ms.Diksha Karmalkar**, PhD scholar, School of Physical and Applied Sciences, Goa University for providing me with her valuable time, unlimited guidance, strong motivation, constant encouragement, helping me to learn new techniques and for all other help required throughout the various stages of my project. I would also like to thank **Mr.Nandesh Kinlekar**, PhD scholar, School of Physical and Applied Sciences, Goa University for helping me to carry out the SQUID measurements and also with the two zone furnace.

I am also thankful to all the staff members of Goa University, School of Physical and Applied Sciences for their support and encouragement.

Last but not the least, I would like to thank my friends and family for their moral support and to God for keeping me in good health throughout the completion of this project.

- **Riya Singh**



# Contents

## 1 Abstract

<b>2</b>	<b>Chapter 1:- Introduction</b>	<b>1</b>
2.1	NASICON Materials . . . . .	1
2.2	History of NASICON Materials . . . . .	2
2.2.1	Li-based NASICON materials . . . . .	2
2.2.2	Na-based NASICON material . . . . .	2
2.3	NASICON based Cathode Materials . . . . .	3
2.3.1	$\text{Na}_3\text{V}_2(\text{PO}_3)_4$ (NVP) . . . . .	3
2.3.2	$\text{Na}_3\text{Fe}_2(\text{PO}_4)_3$ (NFP) . . . . .	5
2.3.3	$\text{Na}_x\text{MM}'(\text{XO}_4)_3$ . . . . .	6
2.3.4	Flourophosphates . . . . .	8
2.3.5	$\text{Na}_3\text{V}(\text{PO}_3)_3\text{N}$ (NVPN) . . . . .	11
2.3.6	$\text{Na}_4\text{Fe}_3(\text{PO}_4)_2(\text{P}_2\text{O}_7)$ (NFPP) . . . . .	12
2.3.7	$\text{Na}_x\text{Fe}_2(\text{PO}_4)(\text{SO}_4)_2$ . . . . .	14
2.4	NASICON based Anode Materials . . . . .	15
2.4.1	$\text{NaTi}_2(\text{PO}_4)_3$ (NTP) . . . . .	15
2.5	NASICON based Solid Electrolytes . . . . .	16
2.6	Objectives:- . . . . .	18
<b>3</b>	<b>Chapter 2:- Methodology and Characterization</b>	<b>19</b>
3.1	Sample Preparations: . . . . .	19
3.2	Characterization of materials . . . . .	23
3.2.1	X-Ray Diffraction . . . . .	23
3.2.2	Electrochemical Impedance Spectroscopy . . . . .	26
3.2.3	DC Polarization technique . . . . .	32
3.2.4	Superconducting QUantum Interference Device (SQUID) . . . . .	33

<b>4</b>	<b>Chapter 3:- Result and Discussion</b>	<b>36</b>
4.1	Phase identification using powder x-ray diffraction . . . . .	36
4.2	Measurement of magnetic property using SQUID magnetometer . . . . .	39
4.3	Phase identification using powder x-ray diffraction . . . . .	40
4.4	Measurement of AC conductivity using Electrochemical impedance (EIS) . . . . .	41
4.5	Measurement of Transport number using DC polarization technique . . . . .	43
<b>5</b>	<b>Conclusion</b>	<b>45</b>
<b>6</b>	<b>References</b>	<b>46</b>

# 1 Abstract

NASICON (Na superionic conductor) based cathode material has gained a lot of attention of researchers in recent years due to its robust 3D network which provides smooth and fast mobility of Na ions, wide operating electrochemical range, good stability. However, they undergo low electronic conductivity and low capacity which limits its use in practical application. This dissertation aims to produce a NASICON based cathode material which is proposed to be a good cathode material. However, to solve the problem we also plan to replace (i) one of the vanadium ion with Fe and (ii) both vanadium ions with  $\text{Fe}_2$  in the general composition  $\text{Na}_3\text{V}_2(\text{PO}_4)_3$ , and study its electronic as well as magnetic properties of the different compositions. Besides, electronic properties of NASICON - based electrolytes were also investigated. Effect on ionic conductivity of the electrolyte materials when sintered in  $\text{N}_2$  and  $\text{O}_2$  atmosphere are also demonstrated in this investigation. The samples prepared was studied using different techniques like PXRD, Electrochemical Impedance Spectroscopy, DC polarization technique and SQUID magnetometer. The phase and structures of the different compositions was characterised using Powder X-ray diffraction.

## 2 Chapter 1:- Introduction

The development and inventions of new technologies like electric vehicles, advancement in personal electronic items like smart phones, smart watches, laptops, tablets and etc. which uses rechargeable batteries which are mainly lithium ion batteries (LIBs), so to fulfill all this requirements there is high demand for lithium ion batteries, but due to some limitations of LIBs like less abundant in nature, comparatively costly, has a high risk of busting at high (during charging), also not applicable for higher temperature range. Due to all this limitations researchers are currently focusing to find an alternating way which is sodium-ion batteries (SIBs) due to its resource abundant, low cost as compare to LIBs and safer to use at high temperature so because of all this reasons sodium-ion batteries is considered to be a good alternative for lithium-ion batteries. To make a sodium battery competitive, an important component in battery is the cathode material. So far three types of sodium-insertion components have been discovered which are layered oxides or sulphides, cyano-perovskites and framework oxides. Among all the above components framework structured NASICON type component is considered as good component for cathode material because it delivers high reversible capacity of  $110 \text{ mAhg}^{-1}$  and a flat voltage plateau of 3.3 - 3.4 V associated with a  $\text{V}^{4+}/\text{V}^{3+}$  redox couple.

### 2.1 NASICON Materials

Sodium-ion batteries (SIBs) have the potential to replace lithium-ion batteries in order to fulfil the growing demands of electrical storage systems because of the high abundance and inexpensive cost of sodium. In order to improve the safety and long-term performance of SIBs for electric energy storage smart grids, Sodium Super Ionic Conductor (NASICON) structured materials has gained a lot of attention recently. These materials have a three dimensional robust framework, feature a quick  $\text{Na}^+$  - ion transport mechanism, high redox potential, and are thermally stable. However, the electrochemical performance is limited by NASICON's low inherent electrical conductivity.

NASICON is an acronym for sodium (Na) super ionic conductor which is a class of solid compound having a general formula  $\text{A}_x\text{M}_y(\text{XO}_4)_n$  where (A = Na, Li, K), (M = transition metal V, Fe, Ni,

Mn etc.), (X = P, Si, S, Mo etc.). It consists of a series of a polyanion tetrahedron unit  $(\text{XO}_4)_n$  and their derivatives, which has strong covalent bond in the  $\text{MO}_x$  polyhedra[1], thus providing it structural and thermal stability which helps in the small volume expansion and phase transition during the insertion/deinsertion of  $\text{Na}^+$  ions.

## 2.2 History of NASICON Materials

### 2.2.1 Li-based NASICON materials

The discovery of Li-based NASICON material was reported by Subramanian et al. [2] in 1986 during the synthesis of  $\text{LiZr}_{2-x}\text{Ti}_x(\text{PO}_4)_3$ ,  $\text{Li}_{1+x}\text{Sc}_x\text{Ti}_{2-x}(\text{PO}_4)_3$ , and  $\text{Li}_{1-x}\text{In}_x\text{Hf}_{2-x}(\text{PO}_4)_3$  using the solid-state reaction method. The ionic conductivity of these compositions was studied using the complex impedance method and the conclusion was found that the ionic conductivity of this compositions was related to the bottleneck size and stoichiometry of the composition, while other researchers also found the existence of 2 phases of transitions in  $\text{LiZr}_2(\text{PO}_4)_3$ , i.e. the  $\text{LiZr}_2(\text{PO}_4)_3$  has a monoclinic phase at room temperature and transforms to a rhombohedral with space group  $\text{R}\bar{3}\text{C}$  at  $25^\circ\text{C}$  -  $60^\circ\text{C}$ . With the increase in temperature to  $280^\circ\text{C}$  the rhombohedral phase is retained with a long range lithium motion which causes a high conduction in Li ions. From 1990 Onwards researchers's main objective was to improve the ionic conductivity of Li-based NASICON via doping or additives methods. A series of  $\text{LiTi}_2(\text{PO}_4)_3$  with  $\text{M}^{3+}$  partial substitution of  $\text{Ti}^{4+}$  was prepared way back in 1990 and researchers found that the increase in the conductivity is due to the densification of 'sintered pellets'[3]. In 2016, Goodenough[4] produced the first all solid state battery performance with rhombohedral solid structured electrolyte  $\text{LiZr}_2(\text{PO}_4)_3$ ,  $\text{LiFePO}_4$  as cathode material which was able to achieve an excellent cycling performance.

### 2.2.2 Na-based NASICON material

In 1968, researchers from the University of Stockholm in Sweden reported  $\text{NaM}_2(\text{PO}_4)_3$  they synthesis various types of compositions like  $\text{NaZr}_2(\text{PO}_4)_3$ ,  $\text{NaTi}_2(\text{PO}_4)_3$  and

$\text{NaGe}_2(\text{PO}_4)_3$  via solid-state method and determine their respective 3 - D X-ray data[5]. A 3 - D network of  $\text{NaM}_2(\text{PO}_4)_3$  crystal was formed by sharing of oxygen atoms, i.e, the  $\text{MO}_6$  and  $\text{PO}_4$  tetrahedral shares the corners oxygen, which was the first report about NASICON materials.

Goodenough and Hong et.al.[4] in 1976 explored the preparation and structural characterisation of  $\text{Na}_{1+x}\text{Zr}_2\text{Si}_x\text{P}_{3-x}\text{O}_{12}$  where  $(0 \leq x \leq 3)$  composition. In this composition it was reported that  $\text{Na}_3\text{Zr}_2\text{Si}_2\text{PO}_{12}$  shows C2/c space group. In this composition each  $\text{PO}_4$  tetrahedra is connected to four  $\text{ZrO}_6$  octahedra whereas each octahedron was connected to six tetrahedra which resulted in the formation of open skeleton structure which helps in fast  $\text{Na}^+$  ion transport. Hence the term NASICON was given because of fast  $\text{Na}^+$  transport in  $\text{Na}_{1+x}\text{Zr}_2\text{Si}_x\text{P}_{3-x}\text{O}_{12}$  which was given by Goodenough and his coworkers. The investigation of  $\text{Na}_{1+x}\text{Zr}_2\text{Si}_x\text{P}_{3-x}\text{O}_{12}$  system by Goodenough lead to the achievement of highest ionic conductivity which was related to the concentration of mobile-ion which was related to the change in the bottleneck due to the variation in  $x$ .

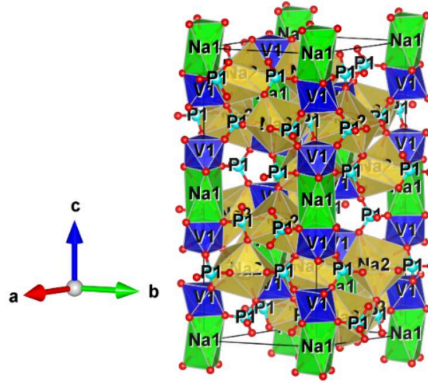
However there was not much development seen in the first decade of 21<sup>st</sup> century, but as the years passed there were some modification taking place to improve its ionic conductivity, and from 2010 the main objective of researchers were to improve the ionic conductivity and modifying the electrode/electrolyte interface, from all theses research work it was clear that Goodenough played a very crucial role in the discovery of NASICON solid-state electrolyte.

## 2.3 NASICON based Cathode Materials

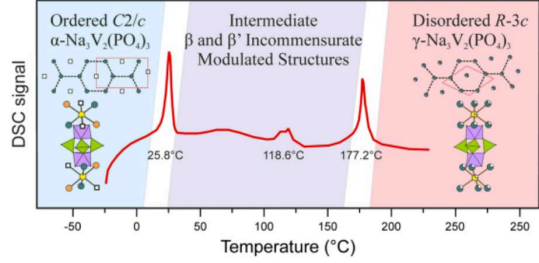
### 2.3.1 $\text{Na}_3\text{V}_2(\text{PO}_3)_4$ (NVP)

The most commonly studied material for SIBs is Vanadium based phosphates with the general formula  $\text{Na}_3\text{V}_2(\text{PO}_3)_4$  as shown in the fig. 1(a)

It has got a stable rhombohedral structure with R-3C space group. In this structure each corners of  $\text{VO}_6$  octahedra is sharing by three  $\text{PO}_4$  tetrahedrons. To form a lantern structure together it constitutes a highly covalent 3-D framework[7]. There are 2 interstitial sites for Na-ion diffusion in NVP that is Na1 and Na2 where one  $\text{Na}^+$  ion is occupies the M1 site with 6-fold coordinate and the other  $\text{Na}^+$  ion occupies the M2 site which is 8-fold coordinate. The combination of 2  $\text{PO}_4$



(a) Structure of  $\text{Na}_3\text{V}_2(\text{PO}_4)_3$



(b) Phase transition of  $\text{Na}_3\text{V}_2(\text{PO}_4)_3$  w.r.t. Temperature[6]

Figure 1: Structure and Phase transition of  $\text{Na}_3\text{V}_2(\text{PO}_4)_3$

tetrahedron and a  $\text{VO}_6$  octahedra as well as due to the curve pathway leads to the 3-D transport of  $\text{Na}^+$  ions. Thus, NVP shows an excellent and stable performance as a half-cell cathode material for SIBs. Researchers are focusing on the practical application in sodium-ion full cell. The experiments conducted by [1] conformed that the Na-ion present only at M2 site and can be extracted during the electrochemical reaction due to the weak bonding of the surrounding oxygen atoms which results into a theoretical capacity of  $117 \text{ mAhg}^{-1}$  and a flat plateau of about 3.3 V, during discharging to low potential ( $\leq 1.5 \text{ V}$ ), an additional  $\text{Na}^+$  can be inserted at M2 sites achieving a fully occupied  $\text{Na}_4\text{V}_2(\text{PO}_4)_3$  state. Therefore  $\text{Na}_3\text{V}_2(\text{PO}_4)_3$  can be used as a cathode as well as anode material. NVP also maintains a good thermal stability upto a temperature of  $450^\circ\text{C}$  even in the discharging state[8]. The crystal structure of a NASICON material varies with temperature which was studied by Chotards group, they demonstrated that  $\text{Na}_3\text{V}_2(\text{PO}_4)_3$  shows 4 distinct crystal structure in the temperature range between  $-30^\circ\text{C}$  to  $225^\circ\text{C}$  which is  $\alpha$ -,  $\beta$ -,  $\beta'$  and  $\gamma$  - NVP as shown in fig. 1(b) respectively[9]. But due to the low intrinsic conductivity of the phosphate framework which has resulted in low cycling stability and low reversible capacity of the NVP. Thus researchers have found a way to overcome this problem this is by carbon coating the NVP which has shown an improved conductivity of the NVP material. Thus apart being used as a cathode material it is also used as anode material due to its low potential of  $\text{V}^{2+}/\text{V}^{3+}$  and  $\text{V}^{1+}/\text{V}^{2+}$  redox couple[10].

### 2.3.2 $\text{Na}_3\text{Fe}_2(\text{PO}_4)_3$ (NFP)

The other class of NASICON material which is widely studied as electrode material is the  $\text{Na}_3\text{Fe}_2(\text{PO}_4)_3$ , it has a robust open framework and shows a theoretical capacity of about  $105 \text{ mAhg}^{-1}$  and a high redox potential of 3.5 V. This compound was first studied by Delmas et al.[11] But the discovery that this compound has 3 different phases at different temperature was studied by Lyubutin et al.[12] in the year 1988.

The phases were  $\alpha$  phase having monoclinic structure at room temperature fig. 2(a) which transforms into superionic rhombohedral having R3C space group fig. 2(b),  $\beta$   $\text{Na}_3\text{Fe}_2(\text{PO}_4)_3$  at 368 K and the last is the  $\gamma$   $\text{Na}_3\text{Fe}_2(\text{PO}_4)_3$  at 418 K temperature.

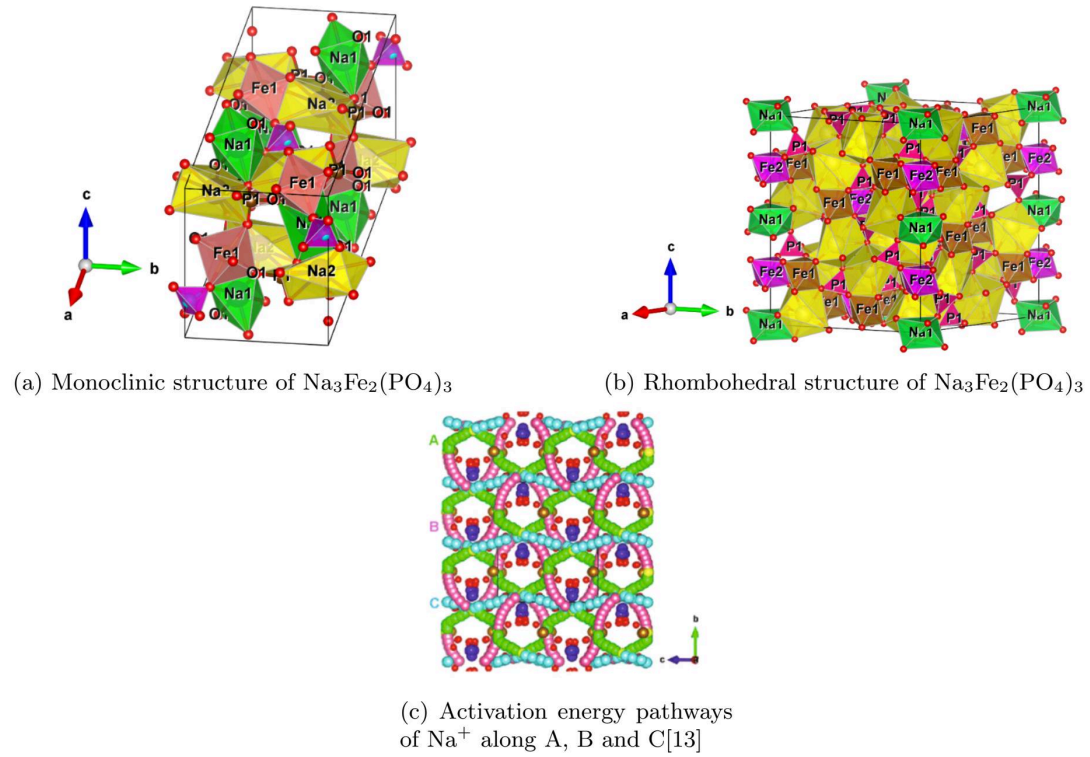


Figure 2: Structure of  $\text{Na}_3\text{Fe}_2(\text{PO}_4)_3$



which was also conformed by Kravchenko and Sigaryov in the year 1992. The crystal structure of  $\text{Na}_3\text{Fe}_2(\text{PO}_4)_3$  has a monoclinic structure with a space group  $\text{C2/c}$  similarly like in the case of NVP. It forms a 3-D open framework in which the  $\text{FeO}_6$  octahedra and  $\text{PO}_4$  tetrahedra are connected by the corner sharing. It has 2 interstitial sites for Na ion which is M1 and M2 discovered by Kuganattam and Chores based on the activation energy of  $\text{Na}_3\text{Fe}_2(\text{PO}_4)_3$  w.r.t. its Na-ion diffusion pathway[14]. Also it was discovered that there are 3 diffusion for  $\text{Na}^+$  having activation energies of 0.44, 0.49 and 2.37 eV for pathways A, B and C respectively as shown in fig. 2(c) [1]. Thus the lowest activation energies of 0.44 and 0.45 were the optimal pathways for Na-ion diffusion, so this makes  $\text{Na}_3\text{Fe}_2(\text{PO}_4)_3$  a potential candidate for cathode materials.

Liu et al.[15] synthesised the monoclinic phase of  $\text{Na}_3\text{Fe}_2(\text{PO}_4)_3$  material for SIBs and reported that it shows a pair of redox peaks of  $\text{Fe}^{3+}/\text{Fe}^{2+}$  at 2.5 V and reversible discharge capacity of  $61 \text{ mAhg}^{-1}$  at 1 C, and shows an excellent rate capability as well as 93% retention of capacity after 500 cycles. However the limitation of NASICON  $\text{Na}_3\text{Fe}_2(\text{PO}_4)_3$  material is that it shows a low discharge capacity as compared to its theoretical capacity, but it can be solved by various methods like carbon coating, elemental doping and nano architecting. Therefore when used as half cell it shows a good performance. Thus we can say that NFP is a potential candidate as an electrode material. But to utilize NFP in practical application more research is needed to improve the performance for its practical application in SIBs.

### 2.3.3 $\text{Na}_x\text{MM}'(\text{XO}_4)_3$

NASICON material where only 1 transition metal ion is present this type of NASICON materials has a general composition of  $\text{Na}_x\text{MM}'(\text{XO}_4)_3$  where  $\text{M} = \text{M}'$  and are called as Single-transition metal NASICON material. However this material has a limited redox reaction which indirectly results in its low energy density. But this problem can be solved in order to make it useful for practical application by replacing 2 different metal ions like  $\text{Na}_x\text{M}_{2-y}\text{M}_y(\text{XO}_4)_3$  where  $\text{M} \neq \text{M}'$  and is called as Mixed transition metal NASICON material also known as binary transition metal NASICON material. It was studied that mixed transition metal phosphates provide multiple electron reaction

and also increases the voltage window, which overall results in the increase in discharge capacity and energy density thus providing a high-performance SIBs. The study of  $\text{Na}^+$  ion intercalation in this NASICON material was done by Tillement et al.[16] in 1992. An example of this type of material is  $\text{Na}_2\text{VTi}(\text{PO}_4)_3$  which shows a theoretical capacity of about  $147 \text{ mAhg}^{-1}$  due to the redox coupling of  $\text{V}^{3+} / \text{V}^{4+}$  and  $\text{Ti}^{4+} / \text{Ti}^{3+}$  NVTP NASICON material shows a rhomboheral crystal structure in which the  $[\text{TiO}_6, \text{VO}_6]$  octahedra forms bond with  $[\text{PO}_4]$  tetrahedra to for a 3-D framework as shown in fig. 3

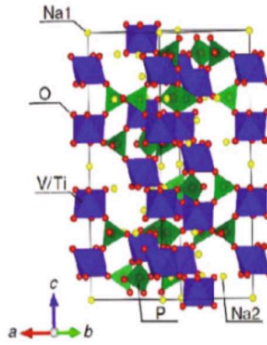


Figure 3: Structure of  $\text{Na}_2\text{VTi}(\text{PO}_4)_3$ [17]

Later Zhou et al.[6] also synthesised  $\text{Na}_4\text{MnV}(\text{PO}_4)_3$  and  $\text{Na}_3\text{FeV}(\text{PO}_4)_3$  by replacing one of the vanadium ion which is more toxic by a highly abundant low-cost element that is Mn and Fe elements of transition metal.  $\text{Na}_3\text{MnV}(\text{PO}_4)_3$  has a single-phase trigonal structure having space group  $R\bar{3}C$  where the 3D network is formed by corner sharing of  $\text{Mn}/\text{VO}_6$  octahedron and the  $\text{PO}_4$  polyhedron respectively. Whereas,  $\text{Na}_3\text{FeV}(\text{PO}_4)_3$  shows a monoclinic structure having space group  $C12c1$ . Similarly different types of binary transition-metal NASICON materials were also studied like  $\text{Na}_4\text{MnCr}(\text{PO}_4)_3$ ,  $\text{Na}_4\text{MnTi}(\text{PO}_4)_3$ . All this materials shows more than 2 electron reaction[1]. The advantage of this type of NASICON Mn, Fe based material is that they provide structural advantage, low-cost and abundant in nature as compared to Vanadium-based materials. However the limitation of these NASICON materials is the reversibility of the redox reaction[1]. Thus researchers are working on this problem to make it high energy density for the practical application of SIBs.

### 2.3.4 Flourophosphates

#### 2.3.4.1 $\text{Na}_3\text{V}_2(\text{PO}_4)_2\text{F}_3$ (NVPF)

In order to improve the performance of NASICON material there is a strategy which is adopted that is to replace one of the  $(\text{PO}_4)$  anion in NVP with  $(\text{PO}_4)\text{F}$ , i.e, NASICON structured flourophosphate having a general composition of  $\text{NVPF}_{2y}\text{O}_{2y}$   $0 \leq y \leq 1$ . Flourine being the most electronegative electron helps in strong bond formation of V-F and V-O in the lattice structure which helps to improve the operating voltage, thermal stability and retention of capacity which improves the electrochemical performance overall[1]. Since NVPF delivers a theroetical capacity of  $128 \text{ mAhg}^{-1}$  and a high theoretical energy density of  $507 \text{ Whkg}^{-1}$ [18], therefore it is the most widely studied NASICON structured vanadium based flourophosphate. The crystal structure of NVPF as reported by Meins et. al.[19] in 1999 is that it shows a tetragonal structure having a space group of  $P 42/m$  n m where  $a = 9.047 \text{ \AA}$ ,  $c = 10.705 \text{ \AA}$  and volume  $V = 876 \text{ \AA}^3$ . The structure of NVPF is such that it forms bond via corner sharing of the two octahedral units ( $\text{V}_2\text{O}_8\text{F}_3$ ) and  $\text{PO}_4$  tetrahedral unit to form a 3-D framework  $(\text{V}_2(\text{PO}_4)_2\text{F}_3)_3$  which has 2 sites for  $\text{Na}^+$  ion diffusion which is Na1 and Na2 along the  $[110]$  and  $[1\bar{1}0]$  directions fig. 4. From studies it has be shown that NVPF

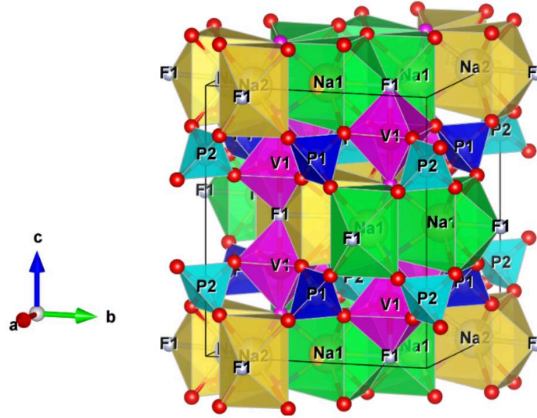


Figure 4: Structure of  $\text{Na}_3\text{V}_2(\text{PO}_4)_2\text{F}_3$

shows better electrochemical performance which not only improves the redox potential voltage as compared to NVP in half-cell SIB. Therefore, it finds its application as a cathode in NIFC, Yan

et al.[20] used NVPF as cathode and carbon as anode to assemble NIFC and was seen that NIFC between the range 2 and 4.3V delivered 11 mAhg<sup>-1</sup> at 0.1C and 77% retention of capacity after 100 cycle also shows a high energy density of 418 Whkg<sup>-1</sup>. The reversible removal Of third NASICON Na-ion from the tetragonal structure helps to increase the energy density of NVPF. Thus NVPF has high redox potential with good electrochemical performance. However it lacks to find a suitable electrolyte which is compatible at high potential due to its high redox potential. Therefore, researchers are working to find a suitable electrolyte for high potential in order to achieve desired performance for its practical application in SIBs.

#### 2.3.4.2 Na<sub>3</sub>(VO)<sub>2</sub>(PO<sub>4</sub>)<sub>2</sub>F (NVOPF)

NVOPF is another class of NASICON material which belongs to the same family of Fluorophosphate having a general composition of NVPF<sub>3-2y</sub>O<sub>2y</sub> where y=1. NVOPF is obtained from oxygenation of NVPF, where one fluorine atom is replaced by an oxygen atom. It shows a V<sup>3+</sup>/V<sup>4+</sup> redox couple and a high voltage window of 3.6-4.1V with a high theoretical capacity of 130 mAhg<sup>-1</sup>[1]. It also shows a strong inductive effect of (PO<sub>4</sub>)F anion[21]. The crystal structure of NVOPF was first explained by Massa et al.[22], which reported that it has a tetragonal structure having a space group 14/mmm where the lattice parameter a = 6.3811 Å and c=10.586 Å, and the unit cell volume V = 431.05 Å<sup>3</sup>. NVOPF forms a 3D crystal structure by the sharing of bioctahedra(V<sub>2</sub>O<sub>10</sub>F) and (PO<sub>4</sub>) tetrahedra which has 2 sites for Na<sup>+</sup> ion diffusion that is Na1 and Na2 at (8h) and (8i) and one F site at (2a) which is different from NVPF as shown in the fig. 5

The electrochemical performance was first studied by Sauvage et al.[23] which shows 2 plateaus at 3.6 V and 4.0 V having a discharge capacity of 87 mAhg<sup>-1</sup> and a poor retention of capacity. So to solve this problem an improved version of NVOPF/C was done by introducing a carbon to it and it was seen that the discharge capacity was improved now to 100 mAhg<sup>-1</sup> but it also showed limited cyclic performance[21]. It was concluded that the battery performance was enhanced due to the presence of carbon and mixed-valence V<sup>3+</sup>/V<sup>4+</sup> which improves the conductivity and electrode mixture. In order to get a long term cycle performance of NVOPF, nanoparticle of Na<sub>3</sub>(VOPO<sub>4</sub>)<sub>2</sub>F was synthesized using a facile solvothermal method at low temperature range[24]. Thus Nano-

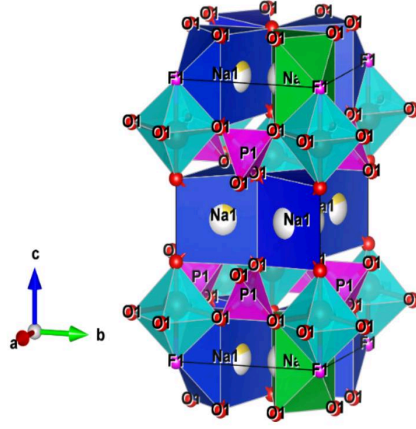


Figure 5: Structure of  $\text{Na}_3(\text{VO})_2(\text{PO}_4)_2\text{F}$

NVOPF showed an initial discharge capacity of  $121.5 \text{ mAhg}^{-1}$  between the range 3 and 4.5 V with an excellent rate capability. It was seen that Nano-NVOPF shows better structure of NVOPF was combined with the 2D nano sheets of  $\text{VO}_2$  which leads to the fast ionic transport and small volume change thus, improving the rate performance. Also due to the flexible structure it is useful in flexible devices. Thus the remarkable ultralong stability and low-cost are the major strength for its use in SIBs. Thus NVOPF delivers a better performance as compared to the other NASICON materials due to the synergic anion effect of fluorine and oxygen atom with different carbon-coated nano porous structure[1]. Thus from the studies we can conclude that NVOPF has got an excellent potential for the practical uses in SIBs.

#### 2.3.4.3 $\text{NVPF}_{-2y}\text{O}_{2y}$

The atoms of the NASICON material having a general composition  $\text{NVPF}_{-2y}\text{O}_{2y}$  becomes unstable at high temperature during the heat treatment due to the presence of carbon and gets transform into NVP,  $\text{Na}_3\text{VF}_6$  and  $\text{V}_2\text{O}_3$ , so the new formed material consists of both vanadium phosphate and fluorophosphate  $\text{Na}_3(\text{VOPO}_4)_2\text{F}$ /NVP which is prepared by carbothermal reduction method[25]. Due to the combination of the stable NVP and high-energy density  $\text{Na}_3(\text{VOPO}_4)_2\text{F}$ , we can achieve long term cyclic stability and high rate capacity. It delivers a discharge capacity of

104 mAhg<sup>-1</sup> at 1 C and 83 mAhg<sup>-1</sup> at very high rate of 100 C having 63% retention for 3000 cycles at 5 C[1]. Also a low-cost Fe-doped NVPF/NVP composite was synthesized by sol-gel method where the high cost and toxic vanadium is replaced with less toxic and low ionic diffusion and electrochemical properties as well[26].

NVPF/NVP showed an initial discharge capacity of 119.8 mAhg<sup>-1</sup> at 0.5 C, it also delivered high energy density of 433 Whkg<sup>-1</sup> at 0.5 C. Thus NVPF/NVP is used in the full cell SIBs as a cathode and CuS as an anode. It was seen that NIFC delivers a high energy density of 162.2 Whkg<sup>-1</sup> and a maximum power density of 1801 Whkg<sup>-1</sup>[1]. Thus all these studies shows that NASICON based fluorophosphate material has high discharge capacity, high theoretical energy density, high redox potential and also has got more structural stability than NVP, this is due to the presence of highly electronegative element which is fluorine, because of their good electrochemical performance in full sodium-ion devices, low-cost and synthesiable via scalable methods. Therefore, NVPF, NVOF and their composites of NASICON material are widely studied.

### 2.3.5 Na<sub>3</sub>V(PO<sub>3</sub>)<sub>3</sub>N (NVPN)

A new class of cathode material that belongs to the family of NASICON material is NVPN having a general composition Na<sub>3</sub>V(PO<sub>3</sub>)<sub>3</sub>N which consists the (PO<sub>3</sub>)<sub>3</sub>N anion group. It has got a cubic crystal structure having a space group of (P 21 3). It forms a 3D network of V(PO<sub>3</sub>)<sub>3</sub>N by the corner sharing of VO<sub>6</sub> octahedra with the three (PO<sub>3</sub>)N tetrahedra which shares the same N atom to form a triphosphate (PO<sub>3</sub>)N fig. 6

It has got 3 sites for Na<sup>+</sup> ion diffusion which is Na1, Na2 and Na3. Due to the presence of nitrogen atom which exerts a strong inductive effect by bonding the V-O bond covalency, which indirectly reduces the gap between the bonding and antibonding orbitals and thus increasing the potential voltage to 4 V[27]. The electrochemical performance and structural changes of NVPN was investigated by Kim et al.[27] It was reported that the diffusion of Na<sup>+</sup> ion from Na2 to Na3 site is fastest as it has got the lowest activation energy of 0.287 eV. It delivers a discharge capacity of 73 mAhg<sup>-1</sup> at 1 C in the voltage window range from 2.5 and 4.25 V having a good rate capability of 84% of capacity at 10 C. The NVPN@NGO composite delivers 78.9 mAhg<sup>-1</sup> at 0.1 C between



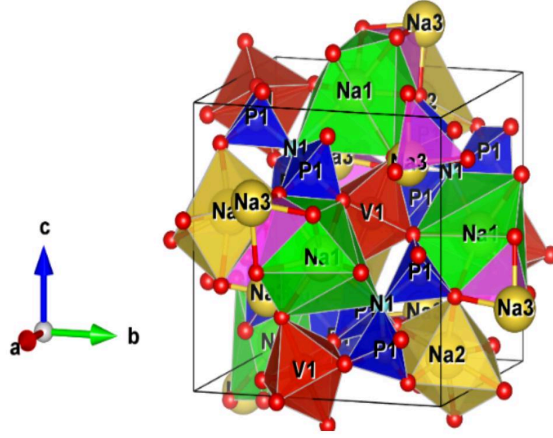


Figure 6: Structure of  $\text{Na}_3\text{V}(\text{PO}_3)_3\text{N}$

the voltage window of 3 and 4.25 V having a rate capacity of  $59.2 \text{ mAhg}^{-1}$  at 30 C, also having a long-term cyclic performance by retaining 79% of the capacity after 5000 cycles at 10 C[1]. Also NVPN@NGO had been subjected to different environment conditions like low temperature, high temperature and air and it was reported that NIFC shows good cyclic performance by retaining 92.3%, 90.3% and 86.4% capacity after 800 cycles at 1 C at low temperature, in air and at high temperature respectively. Thus the full device was studied by using NVPN@NGO as cathode and hard carbon as the anode. Where it showed a capacity retention of about 80% after 150 cycle. But due to the lack of understanding about its crystal structure and diffusion mechanism and lack of research about this material we don't know wheather it can be use as a cathode material in commercial applications of SIBs.

### 2.3.6 $\text{Na}_4\text{Fe}_3(\text{PO}_4)_2(\text{P}_2\text{O}_7)$ (NFPP)

A mixed polyanion material has gained a lot of attention due to its NASICON- type structure with an open 3D framework having a general composition of  $\text{Na}_4\text{Fe}_3(\text{PO}_4)_2(\text{P}_2\text{O}_7)$ . NFPP having a high theoretical capacity of  $129 \text{ mAhg}^{-1}$  and an average voltage value of about 3.2 V have been discovered. It has an orthorhombic crystal structure having space group  $P_n2_1a$ . It consists of 3  $\text{Fe}_2\text{O}_6$  octahedra which are interconnected to 3 tetrahedra ( $\text{PO}_4$ ) to form  $(\text{Fe}_3\text{P}_2\text{O}_{13})$ , along the a

axis fig. 7 In the NFPP there is a formation of large tunnels for  $\text{Na}^+$  ion diffusion along b axis by

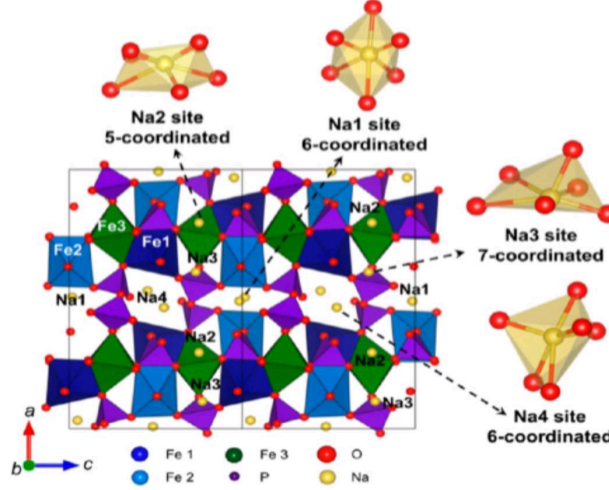


Figure 7: Structure of  $\text{Na}_4\text{Fe}_3(\text{PO}_4)_2(\text{P}_2\text{O}_7)$ [28]

the connection of  $(\text{Fe}_3\text{P}_2\text{O}_{13})_\infty$  and  $\text{P}_2\text{O}_7$  diphosphate along the a axis[29]. The electrochemical performance of this material was first studied by Kim et al.[30] which showed a discharge capacity of  $113.5 \text{ mAhg}^{-1}$  at 0.1 C. NPFF/C was synthesized which showed a high discharge capacity of  $128.5 \text{ mAhg}^{-1}$  at 0.2 C, with an excellent rate capability of  $79 \text{ mAhg}^{-1}$  at 100 C, also it showed 63.5% retention of the initial discharge capacity after 4000 cycles at 10 C[31] in the long term cycle performance. Also Hollow sphere of NFPP/C was reported which showed a discharge capacity of  $107.7 \text{ mAhg}^{-1}$  at 0.2 C and high rate capacity of  $88 \text{ mAhg}^{-1}$  at 10 C which had retention of the initial discharge capacity after 1500 charge/discharge cycle at 10C[32]. This study of mixed polyanion materials suggest that it can be used as cathode material for SIBs since it shows good performance in half-cell battery due to its open 3D structure also the carbon coating enhances the electrochemical performance but since not much work research is being done on this material for full cell, so there is a need for more research to be done in order to make its cyclic performance and rate capability to meet the practical requirement of SIBs.



### 2.3.7 $\text{Na}_x\text{Fe}_2(\text{PO}_4)(\text{SO}_4)_2$

$\text{Na}_x\text{Fe}_2(\text{PO}_4)(\text{SO}_4)_2$  is another class of mixed phosphate explored recently which is made by replacing one  $(\text{PO}_4)$  anion with a highly electronegative sulphate  $\text{SO}_4$  group. This compound was first reported by Shiva et al.[33] as a cathode material for SIBs. It has got a trigonal crystal structure having a space group  $\text{R}\bar{3}\text{C}$ . The electrochemical analysis report revealed that it delivers  $100 \text{ mAhg}^{-1}$  after 50 cycles at  $0.1 \text{ C}$  in a potential window of 2-4 V. It shows an activation energy of about 0.06 eV, which is lower than that of NASICON type sulfate  $\text{Fe}_2(\text{SO}_4)_3$  (0.89 eV)[34], also it delivers  $89 \text{ mAhg}^{-1}$  at  $\text{C}/20$  and 96% capacity retention after 30 cycles at  $\text{C}/5$  at a potential voltage of 3V. The  $\text{NaFe}_2\text{PO}_4(\text{SO}_4)_2$  electrochemical stability was improves by the addition of vanadium and now the composiioon becomes  $\text{NaFe}_{2-x}\text{V}_x\text{PO}_4(\text{SO}_4)_2$ [35]. Now this  $\text{NaFe}_{2-x}\text{V}_x\text{PO}_4(\text{SO}_4)_2$  was synthesized using sol-gel method which has a trigonal crystal structure having a space group  $\text{R}\bar{3}$ . It forms a 3D network which is made up of  $\text{Fe}/\text{VO}_6$  octahedra connected to  $\text{P}/\text{SO}_4$  tetrahedron fig. 8. It shows a discharge capacity of  $> 72 \text{ mAhg}^{-1}$  which shows 96% capacity retention after 50

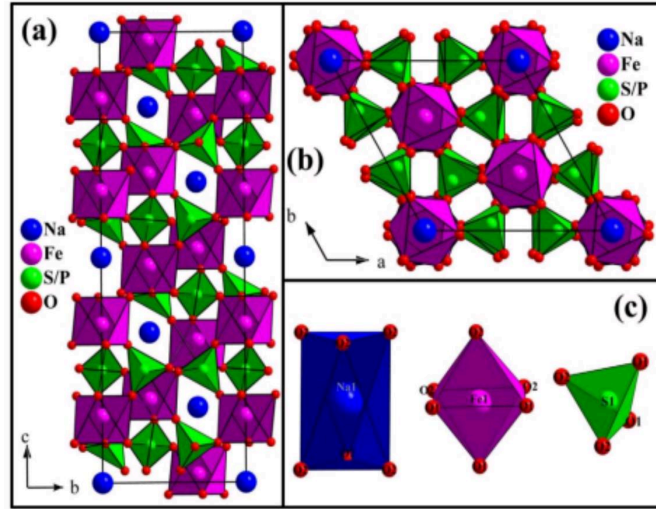


Figure 8: Structure of  $\text{Na}_x\text{Fe}_2(\text{PO}_4)(\text{SO}_4)_2$ [36]

cycles in the potential window between 1.5 and 4.5 V. Thus NFPS has been discovered as a new electrode material in the recent years having mixed phosphate and sulfate anion structures had

been explored in detail. However the discharge capacity and rate performance are comparatively low as compared to other NASICON materials. Thus a lot of research is required in the future in order to improve the electrochemical performance in full cells.

## 2.4 NASICON based Anode Materials

### 2.4.1 $\text{NaTi}_2(\text{PO}_4)_3$ (NTP)

Another class of NASICON material which is widely explored as an anode material for SIBs due to its 3D open framework is NTP having a general composition of  $\text{NaTi}_2(\text{PO}_4)_3$ . It shows a rhombohedral crystal structure, having a space group  $R\bar{3}C$  where the  $\text{TiO}_6$  octahedra and  $\text{PO}_4$  tetrahedra are connected via corner-sharing to form a latern unit fig. 9. It has got 2 interstitial sites

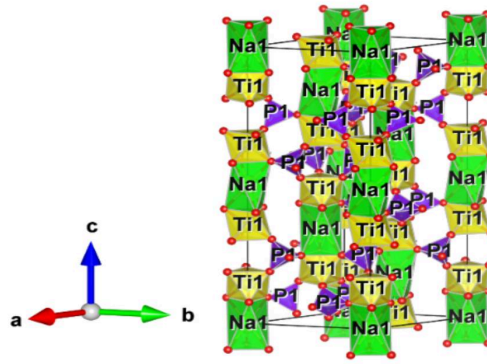


Figure 9: Structure of  $\text{NaTi}_2(\text{PO}_4)_3$

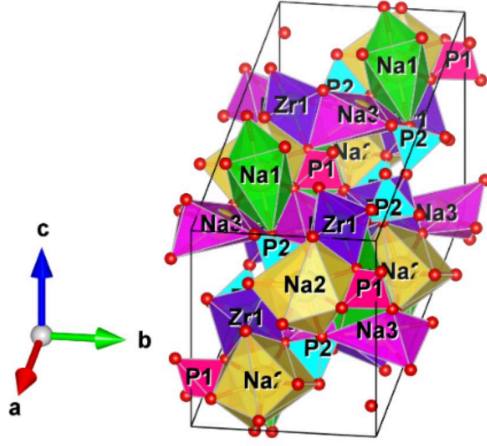
for Na-ion diffusion which is M1 and M2. Thus giving it a structural and thermal stability helping in fast Na ion diffusion and small volume expansion during Na ion (de)intercalation, delivering a large theoretical capacity of  $133 \text{ mAhg}^{-1}$  and long cyclic stability. It was reported that there are two pathways for  $\text{Na}^+$  ion diffusion to take place where the pathway(1) was between the octahedra and tetrahedra along  $[100]$  and pathway(2) was between the 2 tetrahedra along  $[001]$  direction. It shows an activation energy barrier of about  $0.79 \text{ eV}$  along pathway(1) and activation energy of  $0.51 \text{ eV}$  along the pathway(2). That means that  $\text{Na}^+$  ion will prefer the pathway(2). Senguttuvam et al.[37] also reported the presence of a triclinic structure having a space group  $P_1$ . Park et al.[38] reported

that NTP can be used as an anode material for SIBs. It also shows a discharge capacity very close to the theoretical capacity of  $130 \text{ mAhg}^{-1}$ , but NTP shows a poor rate capability because of the low electrical conductivity of phosphate group, which restrict NTP from its practical applications. Due to researchers we can overcome this limitations by carbon coating the material, elemental doping and designing in a 3D porous structure which will increase its surface area. Thus providing fast electronic transport resulting in improving the overall electrochemical performance. NASICON based NTP material shows a good thermal stability, 3D structural framework and having high theoretical capacity of about  $133 \text{ mAhg}^{-1}$ . Thus among all the NASICON materials NTP is considered as a suitable anode material due to its low redox couple, high ionic conductivity and exceptional structural stability which helps in minimum volume change during Na-ion insertion/deinsertion also prevents the formation of SEI on the surface of anode material. Thus when combined with cathode material it shows a comparable performance with LIBs.

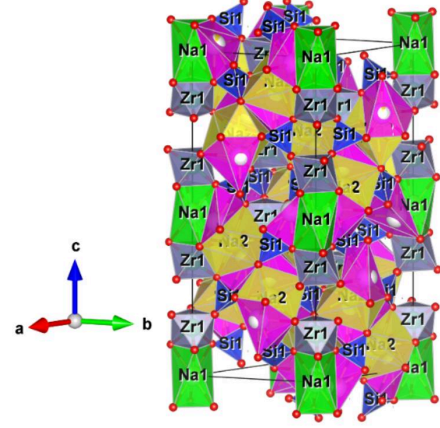
## 2.5 NASICON based Solid Electrolytes

After the discovery of NASICON based solid electrolytes by Goodenough et al.[39],[4] in 1976 lots of research was going on from the last 45 years on this solid electrolytes. It has a general composition of  $\text{Na}_{1+x}\text{Zr}_2\text{P}_{3-x}\text{Si}_x\text{O}_{12}$  ( $0 \leq x \leq 3$ ). It is used as a replacement for liquid electrolyte in SIBs. It has got 2 types of crystal structures which is monoclinic as shown in fig. 10(a) and rhombohedral as shown in fig. 10(b), where the monoclinic has a space group  $\text{C2/c}$   $1.8 \leq x \leq 2.2$  and the rhombohedral crystal structure has space group  $\text{R3C}$ .

$\text{Na}_{1+x}\text{Zr}_2\text{P}_{3-x}\text{Si}_x\text{O}_{12}$  has got a 3D robust framework which is made up of  $\text{ZrO}_6$  octahedra connected by corner sharing to  $(\text{Si/P})\text{O}_4$  tetrahedra. The rhombohedral structure consists of 4  $\text{Na}^+$  diffusion sites, i.e, one Na1 and three Na2 sites, whereas in monoclinic structure the three Na2 sites splits into one Na2 site and two Na3 sites[39],[4]. The ionic conductivity of these material strongly depends on what is the composition and structure of electrolyte.  $\text{Na}_3\text{Zr}_2\text{PSi}_2\text{O}_{12}$  has been reported that it shows an ionic conductivity of  $0.25 \text{ cm}^{-1}$  at  $300^\circ\text{C}$  having an activation energy  $E = 0.29 \text{ eV}$  and  $6.7 \times 10^{-4} \text{ Scm}^{-1}$  at room temperature[1] Jolly et al.[40] studied the phase transition of these material and reported from in situ XRD analysis that monoclinic phase exists at low temperature



(a) Monoclinic structure of  $\text{Na}_{1+x}\text{Zr}_2\text{P}_{3-x}\text{Si}_x\text{O}_{12}$



(b) Rhombohedral structure of  $\text{Na}_{1+x}\text{Zr}_2\text{P}_{3-x}\text{Si}_x\text{O}_{12}$

and a stable rhombohedral phase exists at high temperature. It was also reported that there are two  $\text{Na}^+$  ion migration channel in rhombohedral which is:

1. Na1 - Na3 - Na2 - Na3 - Na1
2. Na2 - Na3 - Na3 - Na2

These migration pathways consists of 3 segments which is Na1 - Na3, Na2 - Na3 and Na3 - Na3 by using intio molecular dynamics (AIMD) simulations[41]. But also it was seen that the Na1 - Na3 channel is dominant as compared to the Na3 - Na3. Thus  $\text{Na}^+$  migration will be more feasible in Na1 - Na3 - Na2 - Na3 - Na1 which will give us high ionic conductivity. Also it was reported that there are 2 types of migration of 2  $\text{Na}^+$  ions at Na1 and Na2 sites one along the same direction and the second one along different direction. The activation energy of  $\text{Na}^+$  is 0.472 eV but here in two  $\text{Na}^+$  ions due to the other conditions like coulomb interaction the activation energy is 0.103 eV along the same direction and 0.242 eV along different direction.

Thus we can say that doping and increasing the  $\text{Na}^+$  ions leads to decrease in activation energy, thus helping to increase the ionic conductivity. Therefore, different doping strategies was taken place in

order to improve the ionic conductivity of  $\text{Na}_{1+x}\text{Zr}_2\text{P}_{3-x}\text{Si}_x\text{O}_{12}$ , so we can say from all these studies that the ionic conductivity of NASICON solid electrolyte can be enhanced by doping, controlled sintering strategies or by porous design structure thus increasing the  $\text{Na}^+$  diffusion sites. Also there is a need of more research in order to increase its ionic conductivity for full cell application of solid state battery.

## 2.6 Objectives:-

The main objectives of this dissertation is:-

1. To synthesis NASICON - based cathode material having a composition  $\text{Na}_3\text{V}_2(\text{PO}_4)_3$  (NVP)
2. To synthesis NASICON - based cathode material having a composition  $\text{Na}_3\text{Fe}_2(\text{PO}_4)_3$  (NFP)
3. To synthesis mixed vanadium - iron based NASICON cathode material having a composition  $\text{Na}_3\text{FeV}(\text{PO}_4)_3$  (NFVP)
4. To study the magnetic properties of NVP, NFP, NFVP
5. To study the electrical conducting properties of NASICON - based electrolyte material having the compositions  $\text{Na}_{3.2}\text{Zr}_2\text{Si}_{2.2}\text{P}_{0.8}\text{O}_{12}$  (parent sample),  $\text{Na}_{3.4}\text{Zr}_{1.9}\text{Zn}_{0.1}\text{Si}_{2.2}\text{P}_{0.8}\text{O}_{12}$  (Zn-doped parent sample),  $\text{Na}_{3.3}\text{Zr}_{1.9}\text{Nb}_{0.1}\text{Si}_{2.4}\text{P}_{0.6}\text{O}_{12}$  (Nb-doped parent sample)
  - (i) when sintered in nitrogen atmosphere ( $\text{N}_2$ )
  - (ii) when sintered in oxygen atmosphere ( $\text{O}_2$ )

## 3 Chapter 2:- Methodology and Characterization

### 3.1 Sample Preparations:

1.  $\text{Na}_3\text{V}_2(\text{PO}_4)_3$  :- The method - 1 and method - 2 [?] and method - 3 [?] which was used to prepare the  $\text{Na}_3\text{V}_2(\text{PO}_4)_3$  sample was prepared using sol-gel method as mentioned on the papers. Sol-gel method is a chemical route used to synthesize materials of high purity at relatively low temperatures, based on wet chemistry processing, that involves the preparation of a sol, the gelation of the sol and the removal of the liquid existing in fine interconnected channels within the gel, below given flowchart shows the preparation methods used to synthesis  $\text{Na}_3\text{V}_2(\text{PO}_4)_3$  sample

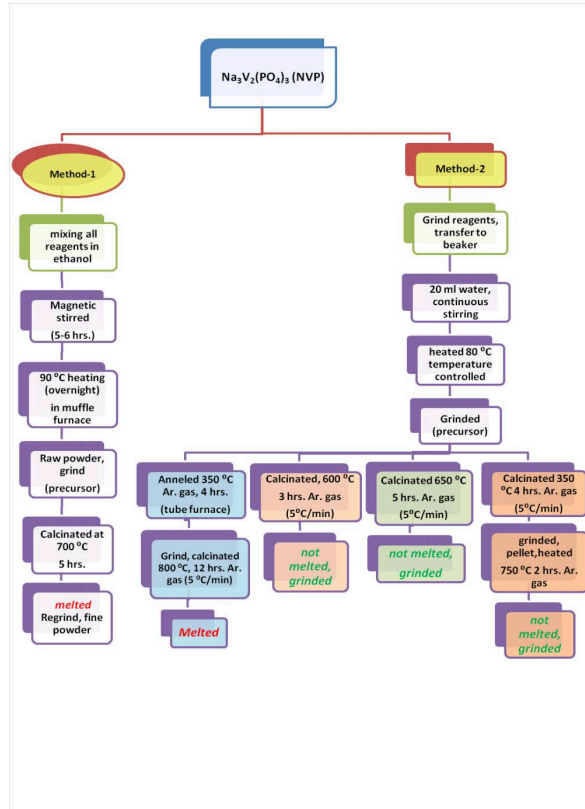


Figure 11: Preparation method - 1 for  $\text{Na}_3\text{V}_2(\text{PO}_4)_3$  sample as referred in paper



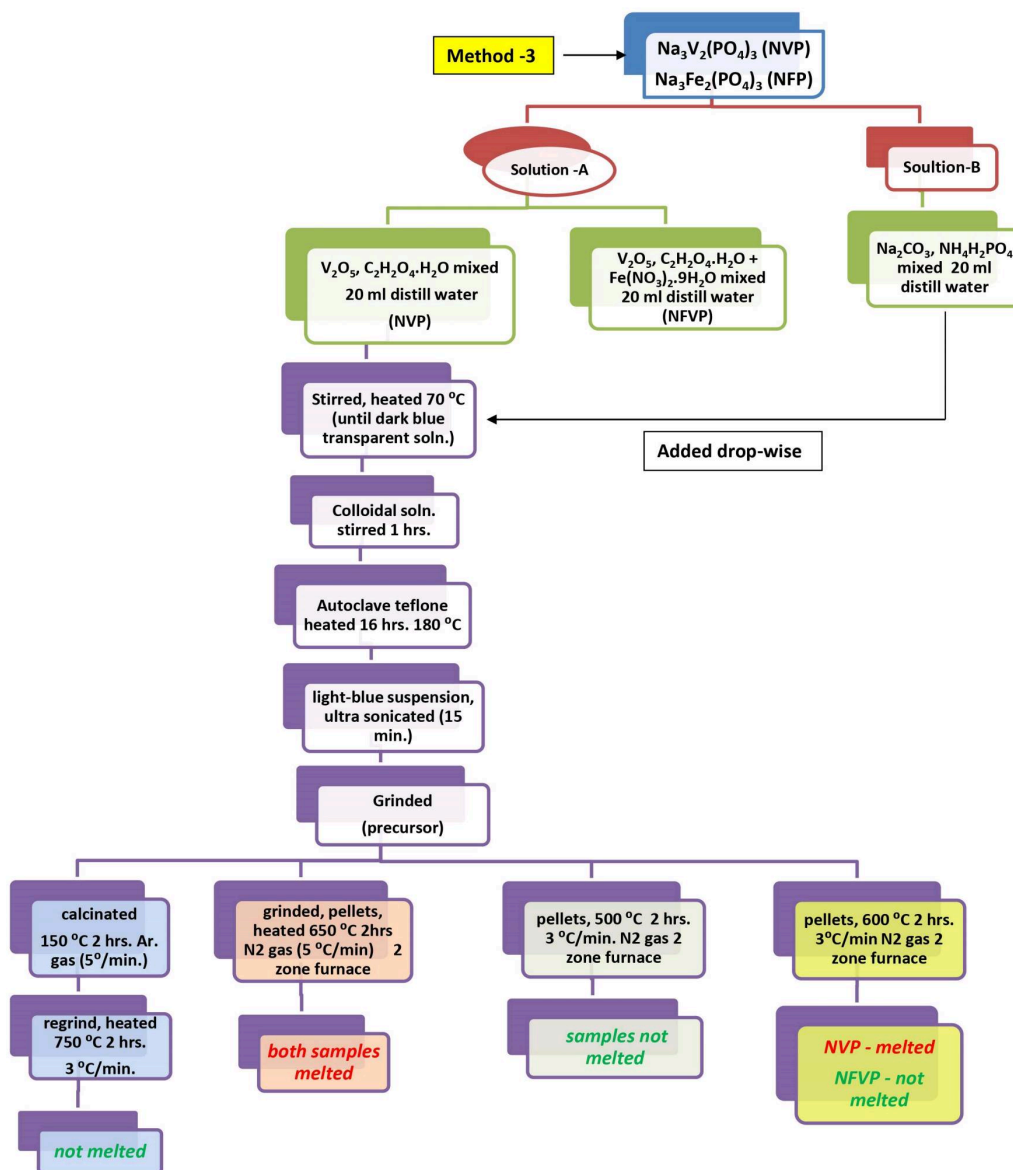


Figure 12: Preparation method - 2 and method - 3 for  $\text{Na}_3\text{V}_2(\text{PO}_4)_3$  sample

## 2. $\text{Na}_3\text{Fe}_2(\text{PO}_4)_3$ : –

$\text{Na}_3\text{Fe}_2(\text{PO}_4)_3$  sample was prepared using solid-state reaction method as mention in paper<sup>1</sup>,

<sup>1</sup>doi.org/10.1016/j.jpowsour.2021.230765

The solid-state reaction route is the most widely used method for the preparation of polycrystalline solids from a mixture of solid starting materials. Solids do not react together at room temperature over normal time scales and it is necessary to heat them to much higher temperatures, often to 1000 to 1500 °C, in order for the reaction to occur at an appreciable rate. The factors on which the feasibility and rate of a solid state reaction depend include, reaction conditions, structural properties of the reactants, surface area of the solids, their reactivity and the thermodynamic free energy change associated with the reaction, below flowchart depicts the method used to synthesis  $\text{Na}_3\text{Fe}_2(\text{PO}_4)_3$  sample

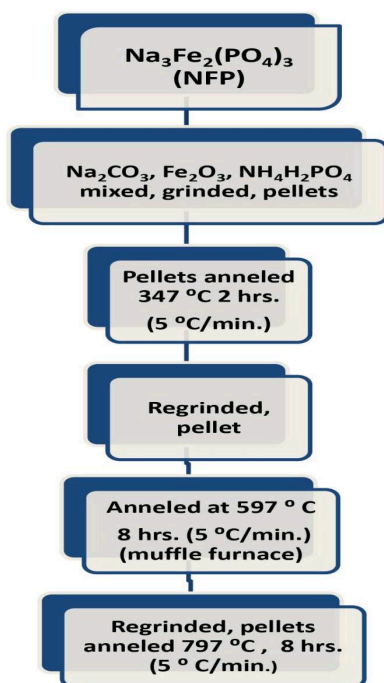


Figure 13: Preparation method for  $\text{Na}_3\text{Fe}_2(\text{PO}_4)_3$  sample



### $\text{Na}_{3.2}\text{Zr}_2\text{Si}_{2.2}\text{P}_{0.8}\text{O}_{12}$ (parent sample), Zn doped and Nb doped parent samples

The  $\text{Na}_{3.2}\text{Zr}_2\text{Si}_{2.2}\text{P}_{0.8}\text{O}_{12}$  (parent sample), Zn-doped<sup>2</sup> and Nb-doped parent samples<sup>3</sup> were also prepared using solid state reaction method as mention in paper.

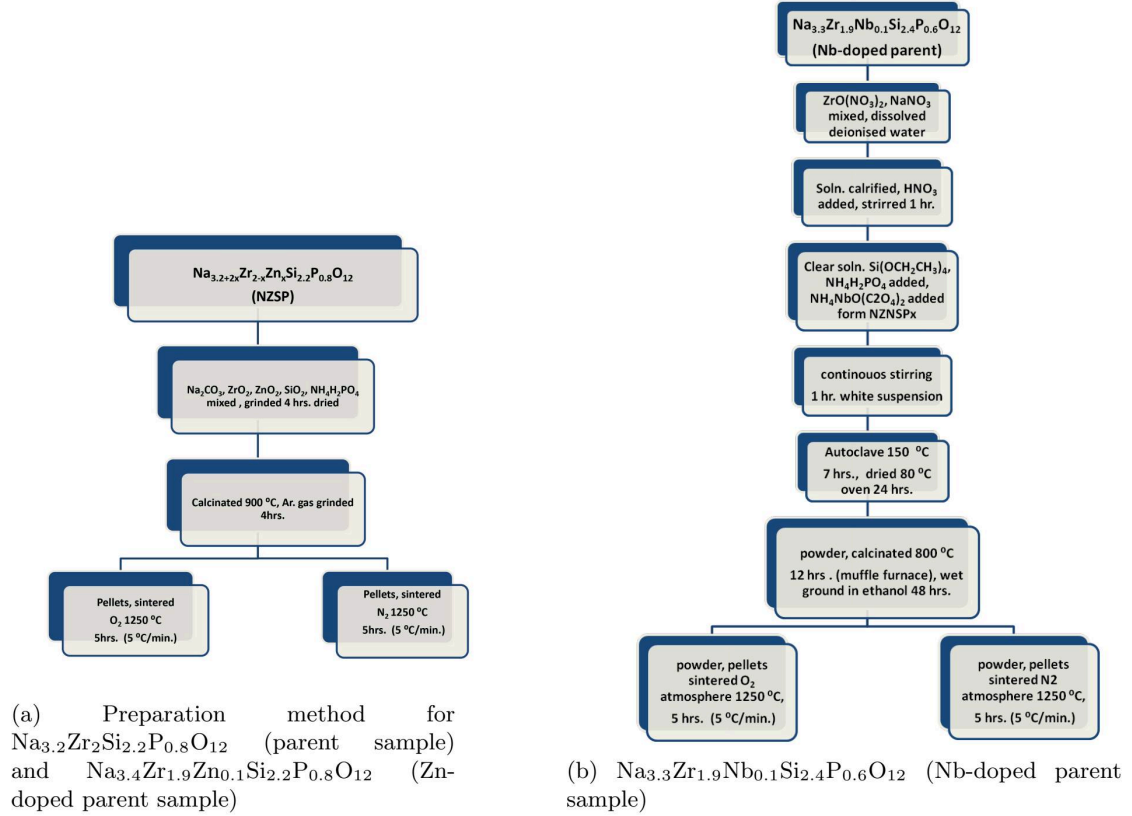


Figure 14: Preparation methods for  $\text{Na}_{3.2}\text{Zr}_2\text{Si}_{2.2}\text{P}_{0.8}\text{O}_{12}$  (parent sample) doped with Zn and Nb samples

<sup>2</sup>doi.org/10.1016/j.jpowsour.2021.230765

<sup>3</sup>doi.org/10.1016/j.jpowsour.2021.230765

## 3.2 Characterization of materials

### 3.2.1 X-Ray Diffraction

X-ray diffraction (XRD) is considered as a powerful, non-destructive technique which is used to characterise the crystalline phase of a material. This technique provides information about material's structure, its phases, the preferred crystal orientation. In this technique a monochromatic beam of X-ray is projected on the sample and the scattered beam from the sample is studied w.r.t. the intensity and the angle of scattering. Therefore XRD plays an important role in revealing the crystalline phase of the material, also it gives information about other structural parameters like the average grain size, its crystallinity, strain and crystal defects or impurity which may be present in the material[?].

#### Principle

In the year 1912, Max Von Laue discovered that materials like crystalline materials can act as a 3-D diffraction grating for X-ray wavelengths in a similar way to the spacing of the planes in a crystal lattice. Therefore a crystalline material having repeating atomic structure can also diffract X-rays. In order to obtain an X-ray diffraction pattern there is a condition which it needs to satisfy i.e, constructive interference of the reflected rays from different planes of the sample should take place in order to obtain an XRD pattern, which will take place when the sample satisfies the Bragg's law<sup>4</sup>.

According to Bragg's law, a crystal is formed by building different layers of atomic planes, where the atomic planes act as a semi-transparent mirror. As shown in fig. (15) Three rays 1, 2, 3 are projected on a crystal planes and their diffracted beams are observed, as seen in the fig. (15) that the incident beam 2 and 3 has to travel an extra distance of  $4d\sin\theta$ . In order for the diffracted beam 1, 2 and 3 to be in phase the distance between ABC must be equal to a whole number multiple of wavelengths i.e,

$$AB = BC = d\sin\theta \dots (1)$$

$$\text{therefore, } ABC = 2 d\sin\theta \dots (2)$$

---

<sup>4</sup>[www.cif.iastate.edu/services/acide/xrd-tutorial/xrd](http://www.cif.iastate.edu/services/acide/xrd-tutorial/xrd)

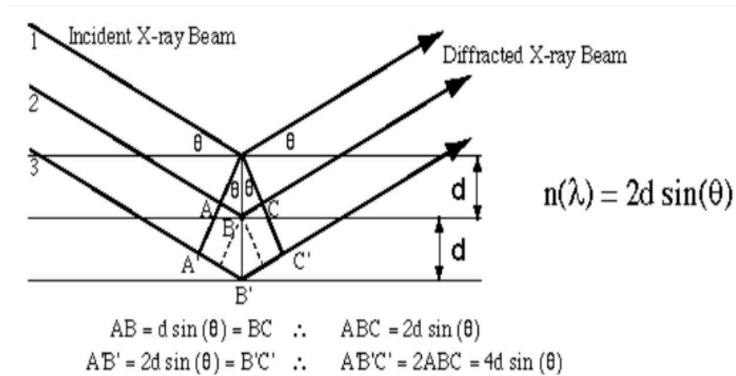


Figure 15: Bragg's reflection <sup>5</sup>

so,  $ABC = n\lambda \dots(3)$

so comparing eq. (2) and (3) we get,

**$n\lambda = 2d \sin \theta$  ← This equation is called as Bragg's law**

This law relates the wavelength ( $\lambda$ ) of electromagnetic radiation to the diffraction angle ( $\theta$ ) and the lattice spacing in a crystalline sample ( $d$ )<sup>6</sup>

So in a crystal there are 2 cases which can take place, if a crystal satisfy Bragg's law which is the reflected rays are in phase with the crystalline material it will give rise to constructive interference and as a result will get a diffraction peaks in the XRD pattern. Whereas, if the Bragg's law is unsatisfied, which means that the reflected rays are not in phase with the crystalline material then destructive interference will take place as a result will not get any diffraction peaks in the XRD pattern.

In practical application the value of  $n$  is kept  $n = 2$ , the  $d$ -spacing will be reduced to half of its original value so for that reason the value of  $n = 1$  for most cases. Since each material has a specific value of  $d$ -spacing helps us to identify the material. Thus the peaks obtained from the diffraction pattern acts as a fingerprint of that material and by comparing the  $d$ -spacing with a standard pattern helps in the identification of the material.

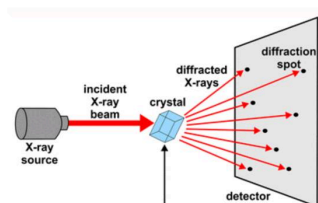
### Working

<sup>6</sup>[www.cif.iastate.edu/services/acide/xrd-tutorial/xrd](http://www.cif.iastate.edu/services/acide/xrd-tutorial/xrd)

An X-ray diffractometer consists of the following three basis elements:

1. X-ray tube
2. Sample holder
3. X-ray detector

Electrons are produced in a cathode ray tube by heating a filament (CuK $_{\alpha}$  radiation  $\lambda = 1.5405 \text{ \AA}$ ) to produce X-rays. These accelerating electrons are then forced to move to a target point by applying a voltage ( $\leq 10 \text{ KV}$ ) resulting in bombarding the target material. But when the electrons have sufficiently enough energy to knock off the inner shell electrons of the target material resulting in the production of characteristic X-ray spectra.



(a) Schematic diagram of x-ray diffraction

<sup>a</sup>[www.cif.iastate.edu/services/acide/xrd-tutorial/xrd](http://www.cif.iastate.edu/services/acide/xrd-tutorial/xrd)



(b) Inside image of Rigaku x-ray diffractometer



(c) Rigaku x-ray diffractometer

Figure 16: X-ray diffractometer

The obtained spectra has several components but the most common one are the  $K_{\alpha}$  and  $K_{\beta}$ . But for most of the diffraction experiments we require a monochromatic beam of X-rays, which is achieved by filtering out all the other wavelengths by the foils or crystal monochrometers (mostly Ni foil). These X-rays beams are then collimated and targeted on the sample. Thus by rotating the sample and detector the reflected X-rays are recorded. Thus a constructive interference occurs resulting a peak to appear when the reflected beam satisfy the Bragg's law. The work of a detector is to record and process the reflected X-ray signal and converting then in count rate, which is then send to a device such as printer or computer monitor<sup>7</sup>.

### 3.2.2 Electrochemical Impedance Spectroscopy

In this technique a small ac signal is applied over a wide range of frequency and measuring the response. This technique is very sensitive to systems which contains several impedance elements, including bulk components and interfaces. Thus making it well - suited technique for devices having multiple components such as battery. In a cell different components and their process takes place at different time scales, having different time constants. Therefore different components can be separated by their respective time constants w.r.t. the frequency using electrochemical impedance spectroscopy technique<sup>8</sup>.

#### Principle

Electrochemical impedance spectroscopy technique is based on the principle of Faraday's law which helps in characterizing the chemical process which is taking place inside a battery in terms of electrical measurement. In this technique during the impedance measurement an AC voltage is applied to the sample at different frequency and the current response is measured. The measured current depends on the mechanism of reaction taking place inside the sample. So when an AC voltage is applied it causes the movement of ions through electrolyte resulting in the formation of new chemical species. Thus we can say that the movement of ions by applying an AC voltage results in the flow of electric current. The applied voltage is of the following form:

<sup>7</sup>West A. R., "Solid State Chemistry and its Applications" John Wiley and Sons, Ltd (2014), 239-241

<sup>8</sup>J. T. S. Irvine et al., "Electroceramics: Characterization by Impedance Spectroscopy", Adv. Mater. 2 (1990) 132-134

$$E(t) = E_o \sin(\omega t) \dots\dots(1)$$

In order to avoid the non - linear response of electrochemical system, the EIS technique measures

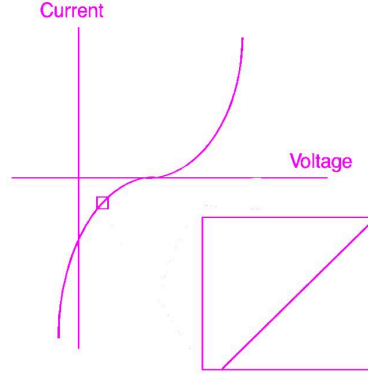


Figure 17: Non - linear response of current vs voltage of electrochemical system

the impedance by applying a small excitation signal so this excitation signal results in a pseudo - linear nature of current vs voltage curve which appears to be linear as shown in fig. (17) but there is a phase shift which is introduced to the current response as given in the below eq.

$$I(t) = I_o \sin(\omega t + \theta) \dots\dots(2)$$

Thus knowing the voltage and current we can now calculate Impedance ( $Z$ ) as:

$$Z = \frac{E(t)}{I(t)} = \frac{E_o}{I_o} \frac{\sin(\omega t)}{\sin(\omega t + \theta)} \dots\dots(3)$$

where  $Z$  can also be written as:

$$Z(\omega) = |Z|e^{i\theta} \dots\dots(4)$$

$$= |Z|(\cos\theta + j\sin\theta)$$

$$= Z' + jZ'' \dots\dots(5)$$

where  $Z'$  is the real part it represents resistance on X - axis,

$Z''$  is the imaginary part which represents reactance on Y - axis,

$\theta = \omega t$  and  $|Z|$  is the modulus of impedance respectively.

In a normal EIS technique a small AC signal is applied (1-10 mV) to the cell so that the system is pseudo-linear by doing so we are eliminating the system's non-linear response to AC voltage which is by measuring the cell current only at the excited frequencies. For a non-linear system the current response shows a harmonic at the excited frequency. A simple definition of harmonics is that it is a

frequency equal to the integral multiplied by fundamental frequency, but in linear system harmonic is absent. So the presence or absence of harmonics can help in identification of the linearity of a system. Some researchers use these harmonic response to estimate the cell's current voltage curve curvature.

The data of EIS is analyzed by fitting it to an equivalent electrical model which are commonly resistors, capacitors and inductors so a basic knowledge of impedance of all this system is useful in analysing the data. Impedance of a circuit depends on the series and parallel combination of elements in it, so for a series impedance circuit the equation is given as:

$$Z_{eq} = Z_1 + Z_2 + Z_3 \dots\dots\dots(6)$$

and for parallel impedance circuit the equation is given as:

$$Z_{eq} = \frac{1}{\frac{1}{Z_1} + \frac{1}{Z_2} + \frac{1}{Z_3}} \dots\dots\dots(7)$$

The analysis of EIS data is carried out by plotting the data in "Nyquist plot" (also called as cole

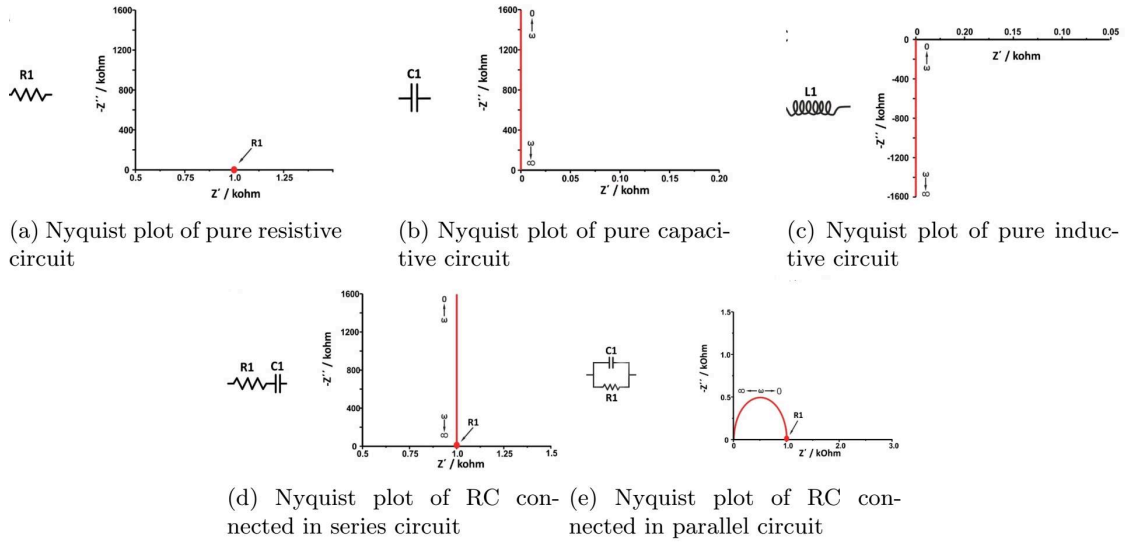


Figure 18: Nyquist plots of various circuit components  
<https://www.gamry.com/application-notes/EIS/basics-of-electrochemical-impedance-spectroscopy/>

- cole plot). In Nyquist plot the negative imaginary part of the impedance ( $-Z''$ ) is plotted on Y - axis and the real part of impedance ( $Z'$ ) is plotted on X- axis for each excitation frequency.

**For a pure resistive circuit** impedance is

$$Z = R + j(0) \dots \dots (8)$$

i.e, the real part is R and the imaginary part is zero, as a result the Nyquist plot shows a single point which lies on the real axis as shown in the fig.(18 (a))

**For a pure capacitive circuit** the impedance is

$$Z = 0 + \frac{1}{j\omega C} \Rightarrow 0 - j \left( \frac{1}{\omega C} \right) \dots \dots (9)$$

where the real part is zero and the imaginary part is inversely proportional to  $\omega C$  and the current is phase shifted w.r.t. voltage by a phase of  $(\theta = +90^\circ)$  as a result the Nyquist plot shows a straight line in the Y - axis fig. (18 (b)).

**For a pure inductive circuit** the impedance is

$$Z = 0 + j\omega L \dots \dots (10)$$

where the real part is zero and the imaginary part is directly proportional to  $\omega L$  therefore the Nyquist plot is a straight line lying in the Y - axis below the real axis because of the phase difference  $(\theta = -90^\circ)$  between the voltage and current as shown in the fig.(18 (c)).

**For a circuit containing a resistor and a capacitor connected in series** the impedance of this circuit is given as:

$$Z(\omega) = R_1 + \frac{1}{j\omega C_1} \Rightarrow R_1 - j \frac{1}{\omega C_1} \dots \dots (11)$$

where  $Z' = R_1$  is the real part and  $Z'' = \frac{1}{\omega C_1}$  is the imaginary part so the Nyquist plot of this circuit is as shown in fig. (18 (d)).

**For a circuit containing a resistor and a capacitor in parallel** the equation of the impedance is given as:

$$Z(\omega) = \frac{1}{(1/R_1 + j\omega C_1)} \Rightarrow \frac{R_1}{1 + j\omega C_1 R_1}$$

$$Z(\omega) = \frac{R_1}{1 + (\omega R_1 C_1)^2} - j \frac{\omega (R_1)^2 C_1}{1 + (\omega R_1 C_1)^2} \dots \dots (12)$$

The above eq. 12 corresponds to a semicircle Nyquist plot as shown in the fig. (18 (e) , 19). In this case at high frequency  $\omega \rightarrow \infty$ ,  $\chi_c \rightarrow 0$  as a result all current passes through the capacitor, this acts as a short circuit as impedance goes to zero, but when  $\omega = \text{low}$ ,  $\chi_c \rightarrow \infty$  so no current can pass through capacitor (C) as a result all the current passes through resistance (R), i.e, the impedance contains a real part  $Z' = R_1$  (when  $\omega = 0$  the current is constant), but at intermediate frequency



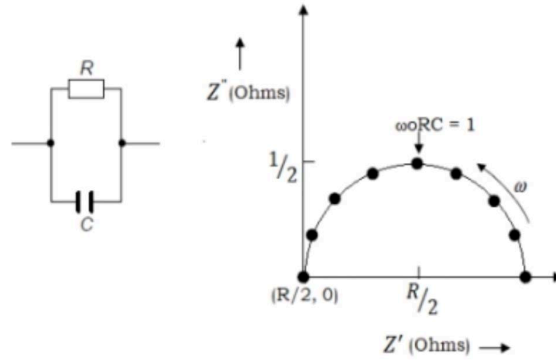


Figure 19: Nyquist plot of RC parallel circuit showing semicircle  
 cite=Cogger, N.D., Evans, N.J. An Introduction to Electrochemical Impedance Measurement,  
 1999 Technical Note, Solartron Analytical Technical Report

the current passes through the capacitor and resistor at the same time and a single characteristic frequency which corresponds to equal value of reactance and resistance is reached ( $\chi_c = R_1$ ) at this frequency the imaginary part of the impedance becomes maximum ( $\omega Z''_{max}$ ), by substituting  $\chi_c = R_1$  in the below eq.

$$\chi = \frac{V_o}{I_o} = \frac{V_o}{V_o \omega C} = \frac{1}{\omega C} = \frac{1}{2\pi f C} \dots \dots (13)$$

time constant of a 'parallel RC' circuit' is given by:

$$\tau = RC \dots \dots (14)$$

$$\text{so, } 1 = \frac{1}{\omega Z''_{max}}$$

$$\text{therefore, } \omega Z''_{max} = \frac{1}{\tau} = \frac{1}{R_1 C_1} \dots \dots (15)$$

where  $\tau$  corresponds to a characteristic time constant of a circuit. Substituting  $R_1 = \frac{1}{\omega Z''_{max}}$  in eq. (12), we get,

$$Z(\omega) = \frac{R_1}{2} - j \frac{R_1}{2} \dots \dots (16)$$

Eq. (16) represents that in an RC parallel circuit  $\tau$  is found when the real and imaginary parts are equal[?].

### Working

In EIS technique an AC voltage is applied across a sample and its response AC current (or vice-versa) is recorded over a wide range of frequency ( $10^{-2} - 10^7$  Hz) arising due to the different

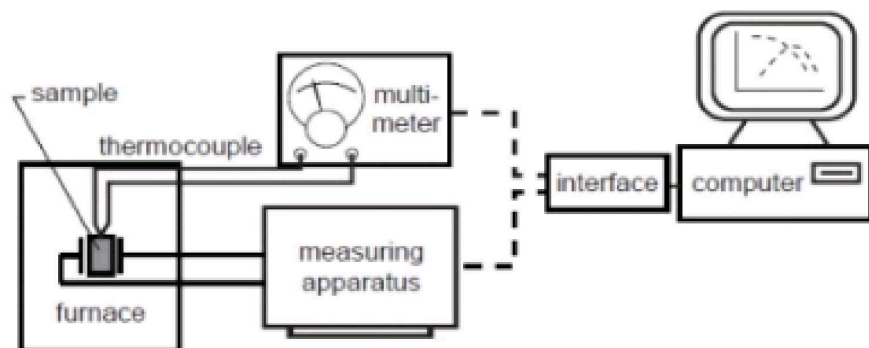


Figure 20: Schematic diagram set-up of electrochemical impedance spectroscopy technique (EIS)  
<https://www.gamry.com/application-notes/EIS/basics-of-electrochemical-impedance-spectroscopy/>



Figure 21: Experiment set-up of electrochemical impedance spectroscopy technique (EIS)

response of grain, grain boundaries, electrodes and ions is determined.

The sample is directly connected to the measuring apparatus which generates the electrical data. The sample is placed in a temperature controlled furnace and the measurements are recorded at different temperatures. In order to verify the exact temperature a thermocouple is placed near the furnace. For data acquisition the measuring system can be directly coupled to a computer by an appropriate interface. In frequency - domain the electrical data of the sample is recorded via frequency response analyzers, impedance analyzers or high precision inductance - capacitance

- resistance meters. So once the data is recorded it can be converted into complex diagrams and then the parameters of equivalent circuit can be fitted to produce the impedance spectra and these circuit parameters can be used to find the physical, chemical process which are taking place inside the material.

### 3.2.3 DC Polarization technique

The transport number gives quantitative information about the ionic and electronic (electrons and holes) contribution to the total conductivity ( $\sigma_T$ ) of a material

$$\text{i.e., } \sigma_T = \sigma_{ion} + \sigma_{electron}$$

where  $\sigma_T$  = total conductivity,  $\sigma_{ion}$  = ionic conductivity and  $\sigma_{electron}$  = electronic conductivity of the material respectively.

The transport number of ion and electron is calculated using the equations given below:

$$\text{Ionic transport no. } \rightarrow t_{ionic} = \frac{I_{total} - I_{electron}}{I_{total}} \dots\dots(1)$$

$$\text{Electronic transport no. } \rightarrow t_{electronic} = \frac{I_{total} - I_{ionic}}{I_{total}} \dots\dots(2)$$

Closer the value of transport no. to unity, higher the contribution to the conductivity of  $t_{ion}$  /  $t_{electron}$  to the material. For electrolyte materials the contribution of  $t_{ion}$  is close to unity and  $t_{electron}$  contribution is negligible as compared to  $t_{ion}$ . One of the most important technique which is used to determine the transport no. is the "DC Polarization technique" (Wagner's method). The most convenient and widely used method which was suggested by Wagner in 1957, which is used to measure the ionic/electronic transport no. in various solid electrolyte materials.<sup>9</sup>

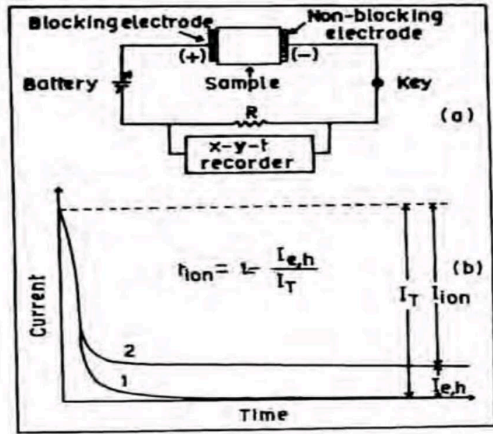
#### Working principle

For the measurement of transport no. cylindrical pellets of the samples was silver pasted to provide better electrical contact. A constant dc voltage ( $V = 0.8 \text{ V}$ ) is applied across the sample which causes the polarization (separation of charges) of the sample, and the response of the current is recorded as a function of time. A graph of current vs time is plotted which helps in the determination of transport no. using the formula given in eq.(1) and eq.(2) respectively.

---

<sup>9</sup>Indian Journal of Pure and Applied Physics Vol. 37. April 1999. pp. 294-301

Thus for solid electrolyte the ionic transport no. is close to unity, so one can say that in electrolyte materials the ionic contribution is more as compared to electronic contribution to the total conductivity of the material.



(a) Schematic diagram of DC polarization technique <sup>a</sup>

<sup>a</sup>Indian Journal of Pure and Applied Physics Vol. 37. April 1999. pp. 294-301



(b) Experiment set-up of DC polarization technique

Figure 22: DC polarization technique

### 3.2.4 Superconducting QUantum Interference Device (SQUID)

SQUID magnetometer is considered to be one of the most effective and sensitive technique to measure the magnetic properties of a material. It is the only method that allows us to directly measure the magnetic moments of a material in an absolute unit. It is a very sensitive magnetometer that is used to measure extremely weak magnetic fields based on superconducting loops containing Josephson junctions. Since squid is very sensitive we can obtain a resolution of the order of  $10^{-8}$  emu. This makes squid a very useful technique for those samples that shows low magnetisation when an external magnetic field is applied to it.

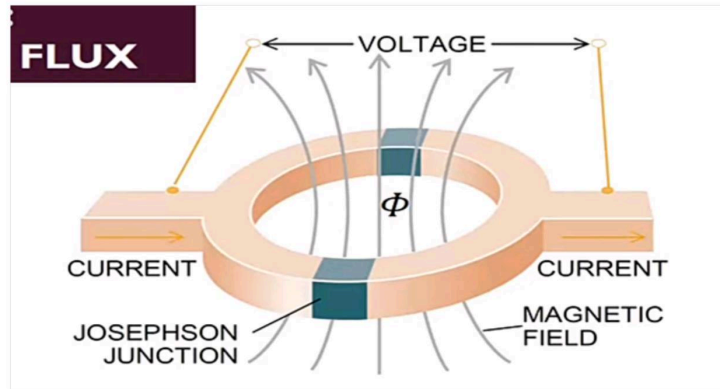


Figure 23: Superconducting loop with 2 josephson junction

### Working principle

SQUID works on the principle of superconductivity, Josephson junction, and magnetic flux quantization. In a superconductor there is tunneling of superconducting electrons (cooper pair electrons) through an extremely thin insulating gap between the two superconductors where the gap is known as the Josephson junction as shown in the fig. (24))

A SQUID magnetometer consists of the following components:

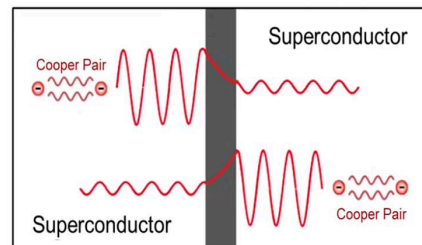
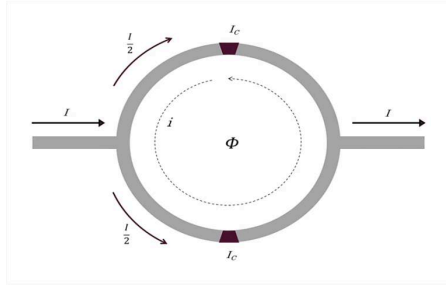


Figure 24: Tunneling of cooper pairs from one superconductor to another through thin insulating gap

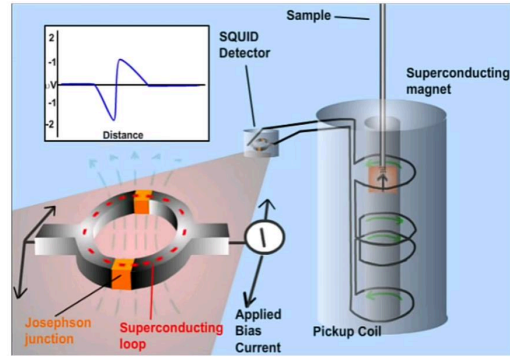
A superconducting measuring current flows across the ring such that the total supercurrent is divided into two parts which then passes through the two identical josephson junctions. So when we apply an external magnetic field, a magnetic flux  $\phi$  goes through the superconducting loop and as a result it induces a persistent current which is based on "Faraday's law", now this induced current is in the

direction of the current flowing through one part of the Josephson junction  $\frac{I}{2}$  in the superconducting loop and is in the opposite direction of current flowing through the superconducting loop in the other half part of the loop  $\frac{I}{2}$ . So because of this the current after passing the Josephson junction there is a phase shift in the current fig. (25(a)). As we know that magnetic flux passing through a superconducting loop is quantized and because of these the current after passing through the Josephson junction when they interfere there is a phase shift in the currents<sup>10</sup>

When a magnetic material is placed in the superconducting loop containing Josephson junction,



(a) Splitting of current at the 2 Josephson junctions



(b) Set-up of SQUID magnetometer

Figure 25: Superconducting loop and set-up of SQUID magnetometer

and the sample is made to move up and down (vibrate) it produces an alternating magnetic flux in the pick-up coil. The magnetic signal of the sample is obtained by the superconducting pick-up coils which have 4 windings. This coil together with the SQUID antenna contributes to the whole superconducting circuit. Then this magnetic signal from the sample is transferred to an rf SQUID device which is located away from the sample in the liquid helium bath. This device acts as a magnetic flux-to-voltage converter. Where this voltage is then amplified and read out by the magnetometer's electronics fig. (25(b))<sup>11</sup>.

<sup>10</sup>S700X SQUID Magnetometer User Manual Version 0.995

<sup>11</sup>S700X SQUID Magnetometer User Manual Version 0.995



## 4 Chapter 3:- Result and Discussion

### 4.1 Phase identification using powder x-ray diffraction

#### 4.1.1 $\text{Na}_3\text{V}_2(\text{PO}_4)_3$ (NVP) sample

The x-ray powder diffraction data was collected for  $\text{Na}_3\text{V}_2(\text{PO}_4)_3$  (NVP) sample at room temperature in the range of  $10^\circ \leq 2\theta \leq 80^\circ$  at the scan speed of  $5^\circ/\text{min}$ . using monochromatic  $\text{Cu K}\alpha$  radiation having  $1.54 \text{ \AA}$  wavelength, fig. (26) shows the xrd diffraction plot of the NVP sample which was prepared using various methods.

The calculated Bragg positions of NVP sample are also shown in fig. (26). By comparing the

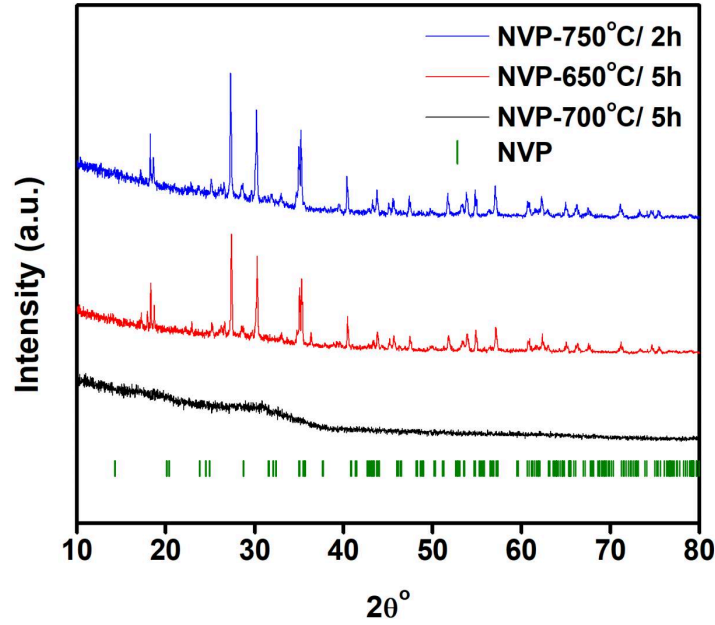


Figure 26: Graph of NVP sample prepared by different methods

By comparing the Bragg position with the observed diffraction peaks we can say that the  $\text{Na}_3\text{V}_2(\text{PO}_4)_3$  phase was not formed. This can be because every time the sample was getting melted at the final heat treatment and leading to an amorphous phase formation

#### 4.1.2. $\text{Na}_3\text{FeV}(\text{PO}_4)_3$ (NFVP) sample

The  $\text{Na}_3\text{FeV}(\text{PO}_4)_3$  sample was synthesized as mention in method - 3 it was observed that the sample did not melt at the final heat treatment, however comparing the xrd pattern of  $\text{Na}_3\text{FeV}(\text{PO}_4)_3$  sample observed with its calculated Bragg's peaks fig. (27) which implies that the expected phase was not formed.

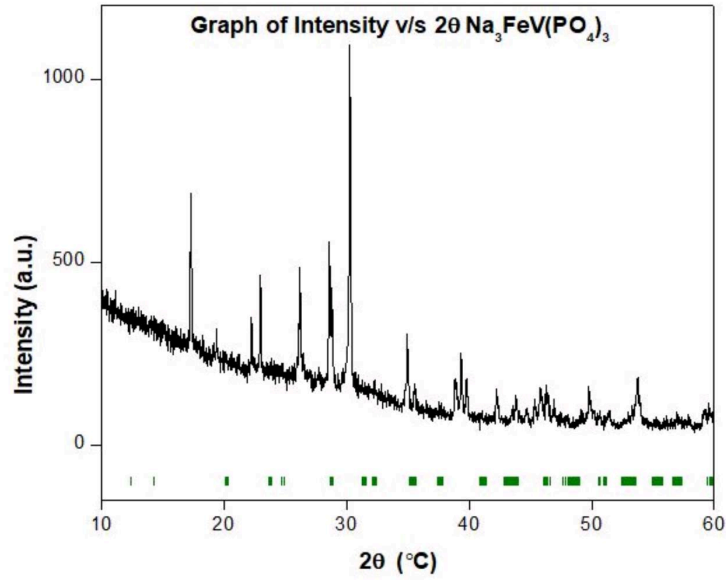
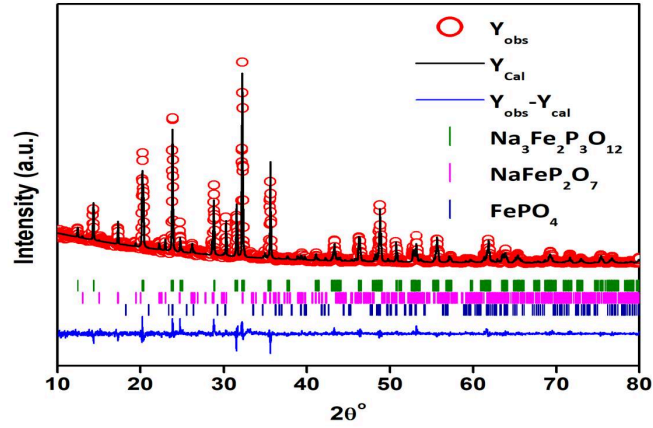


Figure 27: Observed xrd plot vs the calculated Bragg's peak of  $\text{Na}_3\text{FeV}(\text{PO}_4)_3$  sample



#### 4.1.3 $\text{Na}_3\text{Fe}_2(\text{PO}_4)_3$ (NFP) sample

The  $\text{Na}_3\text{Fe}_2(\text{PO}_4)_3$  (NFP) sample was synthesized and it was observed that after the final heat treatment the sample did not melt, fig. (28 (a)) shows the observed and calculated XRD pattern of  $\text{Na}_3\text{Fe}_2(\text{PO}_4)_3$  sample with the NASICON Bragg phase. By comparing both the plots we can conclude that the  $\text{Na}_3\text{Fe}_2(\text{PO}_4)_3$  sample's monoclinic C12/ c1 phase was formed with minor impurity phases of  $\text{NaFeP}_2\text{O}_7$  and  $\text{FePO}_4$  phases as shown in fig. (28(a)). The lattice parameters of the obtained phases was refined using fullproof software and fig. (28(b)) shows the refined lattice parameters



(a) Rietveld XRD pattern of NFP sample

Phases	Space group	Refined lattice parameters	Phase fraction
$\text{Na}_3\text{Fe}_2(\text{PO}_4)_3$ Monoclinic	C 1 2/c 1	$a = 15.137 \text{ \AA}$ , $b = 8.724 \text{ \AA}$ , $c = 8.797 \text{ \AA}$ , $\alpha = \gamma = 90^\circ$ , $\beta = 125.145^\circ$	84.54 %
$\text{NaFeP}_2\text{O}_7$ Monoclinic	P 1 21/c 1	$a = 7.323 \text{ \AA}$ , $b = 7.902 \text{ \AA}$ , $c = 9.572 \text{ \AA}$ , $\alpha = \gamma = 90^\circ$ , $\beta = 111.822^\circ$	15.30 %
$\text{FePO}_4$ Monoclinic	P n m a	$a = 9.735 \text{ \AA}$ , $b = 6.112 \text{ \AA}$ , $c = 4.720 \text{ \AA}$ , $\alpha = \gamma = \beta = 90^\circ$	0.16 %

(b) Refined parameters of the phases

Figure 28: XRD plot and refined lattice parameter of NFP sample

## 4.2 Measurement of magnetic property using SQUID magnetometer

To measure the magnetic property of  $\text{Na}_3\text{Fe}_2(\text{PO}_4)_3$  sample, the sample was subjected to an applied external magnetic field (H) in the range 0 to 2 Tesla and the resulted magnetic moment was observed at constant room temperature ( $T = 300 \text{ K}$ ).

Hence a graph of magnetic moment v/s applied magnetic filed was plotted as seen in fig. (29) from

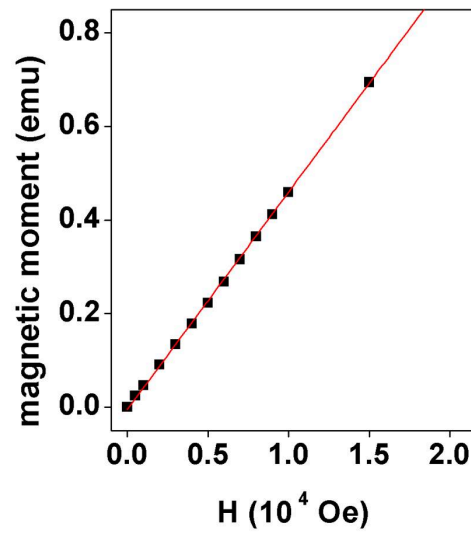


Figure 29: magnetic moment v/s applied magnetic filed graph of  $\text{Na}_3\text{Fe}_2(\text{PO}_4)_3$  sample

the graph we can see that  $\text{Na}_3\text{Fe}_2(\text{PO}_4)_3$  sample graph of magnetic moment v/s applied magnetic field shows a linear relationship, so we can say that  $\text{Na}_3\text{Fe}_2(\text{PO}_4)_3$  sample shows paramagnetic property at room temperature. The ground state magnetic property will be determined by measuring susceptibility at low temperatures. But we can conclude that NFP sample shows a paramagnetic property at room temperature as shown in fig. (29)

### 4.3 Phase identification using powder x-ray diffraction

The phase identification of  $\text{Na}_{3.2}\text{Zr}_2\text{Si}_{2.2}\text{P}_{0.8}\text{O}_{12}$  (parent sample),  $\text{Na}_{3.4}\text{Zr}_{1.9}\text{Zn}_{0.1}\text{Si}_{2.2}\text{P}_{0.8}\text{O}_{12}$  (Zn-doped parent sample) and  $\text{Na}_{3.3}\text{Zr}_{1.9}\text{Nb}_{0.1}\text{Si}_{2.4}\text{P}_{0.6}\text{O}_{12}$  (Nb-doped parent sample) was done using powder x-ray diffraction and fig. (30) shows the xrd plot of the electrolyte samples.

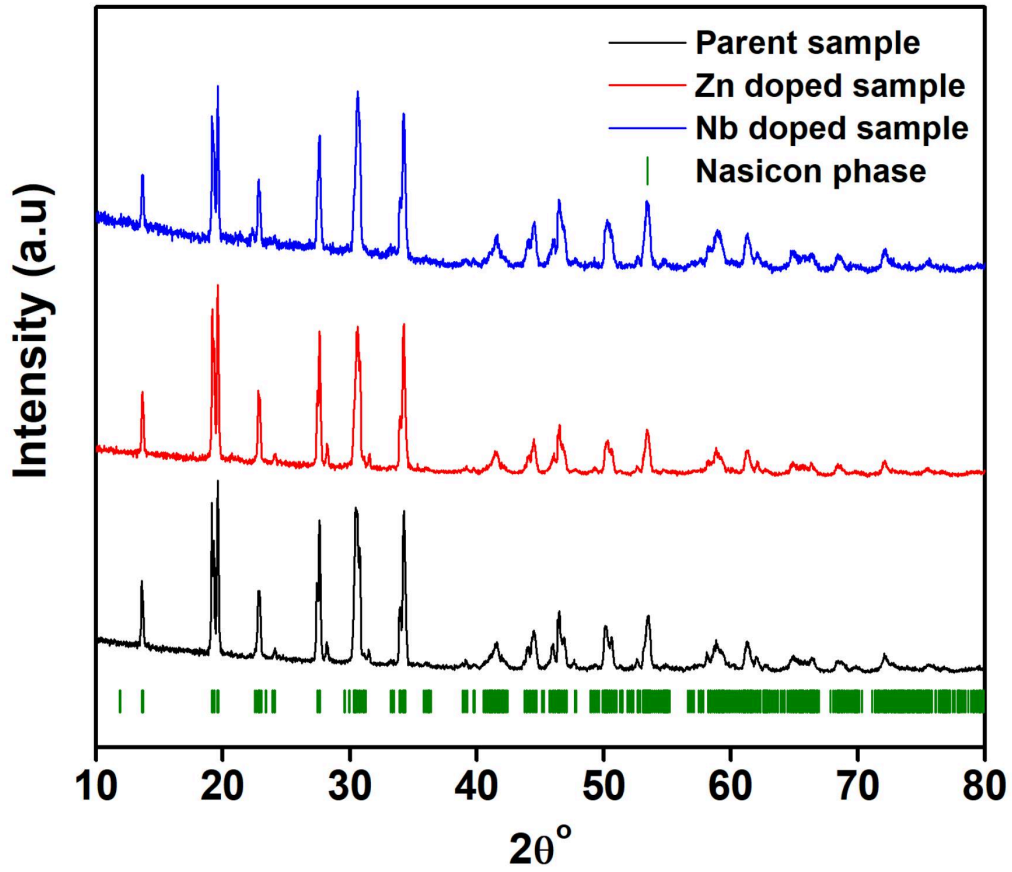


Figure 30: Graph of Intensity vs  $2\theta$  of  $\text{Na}_{3.2}\text{Zr}_2\text{Si}_{2.2}\text{P}_{0.8}\text{O}_{12}$  (parent sample),  $\text{Na}_{3.4}\text{Zr}_{1.9}\text{Zn}_{0.1}\text{Si}_{2.2}\text{P}_{0.8}\text{O}_{12}$  (Zn-doped parent sample) and  $\text{Na}_{3.3}\text{Zr}_{1.9}\text{Nb}_{0.1}\text{Si}_{2.4}\text{P}_{0.6}\text{O}_{12}$  (Nb-doped parent sample) electrolyte samples

#### 4.4 Measurement of AC conductivity using Electrochemical impedance (EIS)

The AC conductivity of the NASICON based electrolyte materials was determined using the electrochemical impedance spectroscopy. Before taking the measurements, the cylindrical pellets of the samples were coated with commercial silver paste on the top and bottom surface of the pellets. The pellets was silver pasted to provide electrical contact. The impedance data was recorded for the  $\text{Na}_{3.2}\text{Zr}_2\text{Si}_{2.2}\text{P}_{0.8}\text{O}_{12}$  (parent sample),  $\text{Na}_{3.4}\text{Zr}_{1.9}\text{Zn}_{0.1}\text{Si}_{2.2}\text{P}_{0.8}\text{O}_{12}$  (Zn-doped parent sample) and  $\text{Na}_{3.3}\text{Zr}_{1.9}\text{Nb}_{0.1}\text{Si}_{2.4}\text{P}_{0.6}\text{O}_{12}$  (Nb-doped parent sample) pellets sintered in  $\text{O}_2$  and  $\text{N}_2$  atmospheres at room temperature ( $30^\circ\text{C}$ ) in the frequency range 10 Hz to 8 MHz, fig. (31) shows the Nyquist plot of the parent, Zn-doped parent and Nb-doped parent samples sintered in  $\text{O}_2$  and  $\text{N}_2$  atmosphere

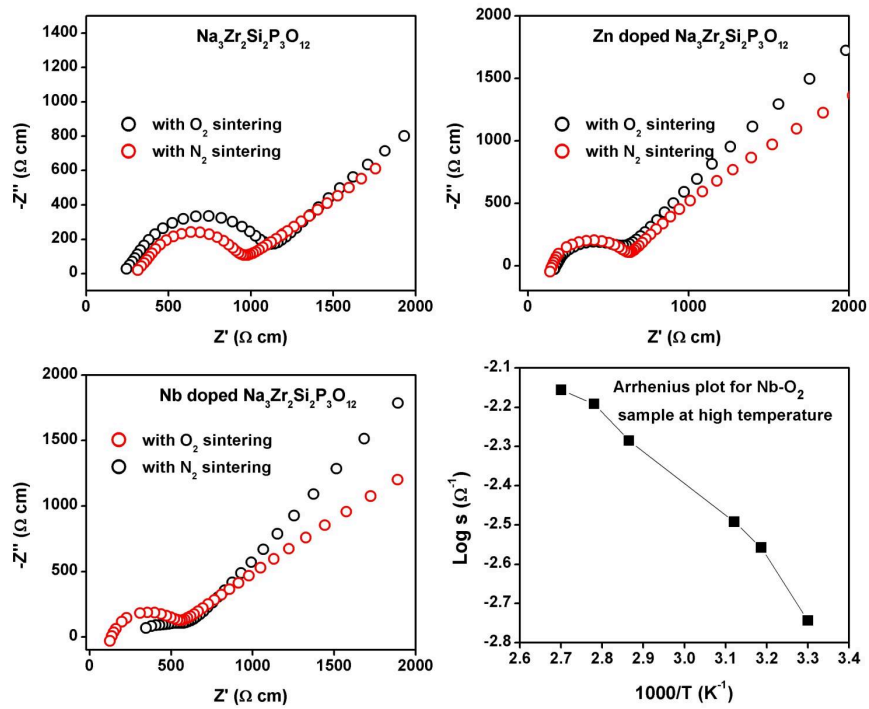


Figure 31: Nyquist plot of all the samples along with arrhenius plot for Nb sample at high temperatures

As we can see in the fig. (31) the semicircle at high frequency is due to the contribution of bulk and grain boundary of the sample and the spike at low frequency is due to the contribution of the electrode-electrolyte interface resistance. Fig. (32) shows the table of conductivity values of samples at room temperature and it was observed that Nb-doped parent sample sintered in O<sub>2</sub> atmosphere displayed higher ionic conductivity at room temperature as compared to other electrolyte samples. So Nb-doped parent sample was subjected to higher temperature range from room temperature to 100 ° C to know what happens to the ionic conductivity of the sample at higher temperature, fig. (31) shows the Arrhenius plot of Nb-doped parent sample from 30 ° C to 100 ° C

Samples	Conductivity at 30 °C (mS/cm)	
	O <sub>2</sub> atmosphere	N <sub>2</sub> atmosphere
Parent sample	0.89	1.03
Zn – doped parent sample	1.63	1.59
Nb – doped parent sample	1.80	1.69

Figure 32: Conductivity value of samples at T = 30 ° C

It was observed that the ionic conductivity of the sample was high for Nb-doped parent sample. To find the conductivity of different electrolyte samples, we find the value of resistance R from the complex plane plots and substitute it in the equation given below:

$$\sigma = \frac{1}{R} \frac{l}{A}$$

where R = resistance, l= thickness of the pellet and A = area of the sample. and the Arrhenius graph was plotted from 30 °C to 100 ° C as shown in the fig. (31). Which implies that as the temperature increases from 30 ° C to 100 ° C the ionic conductivity of the sample also increases, this can be due to the reduction in the grain and grain boundary resistance as the temperature increases.

#### 4.5 Measurement of Transport number using DC polarization technique

The DC polarization of the NASICON based electrolyte materials which are  $\text{Na}_{3.2}\text{Zr}_2\text{Si}_{2.2}\text{P}_{0.8}\text{O}_{12}$  (parent sample),  $\text{Na}_{3.4}\text{Zr}_{1.9}\text{Zn}_{0.1}\text{Si}_{2.2}\text{P}_{0.8}\text{O}_{12}$  (Zn-doped parent sample) and  $\text{Na}_{3.3}\text{Zr}_{1.9}\text{Nb}_{0.1}\text{Si}_{2.4}\text{P}_{0.6}\text{O}_{12}$  (Nb-doped parent sample) was determined using the DC polarization method. Before the measurement the pellets of the samples were silver pasted on the top and bottom for better electrical conductivity.

A voltage of 0.8V was applied to the sample and the response of current was noted as a function

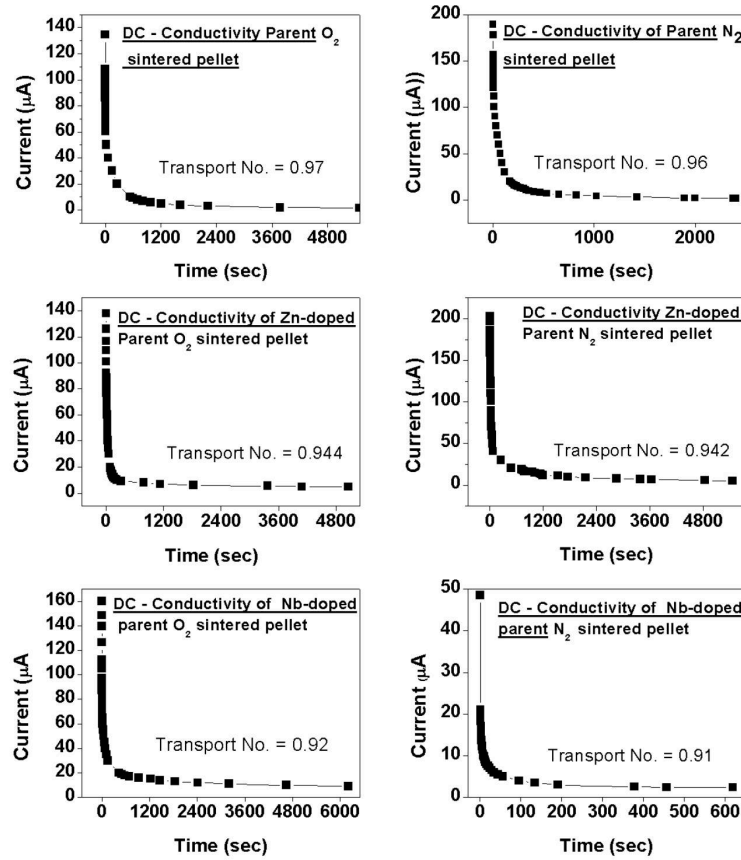


Figure 33: Graph of DC conductivity measurement of all samples

of time for all the samples. Thus a graph of current v/s time was plotted and the transference number was determined from the graph using the formula

$$\text{Transference No.} = \frac{I_{\text{total}} - I_{\text{electronic}}}{I_{\text{total}}}$$

Samples	Transport no. at 30 °C	
	O <sub>2</sub> atmosphere	N <sub>2</sub> atmosphere
Parent sample	0.97	0.96
Zn – doped parent sample	0.944	0.942
Nb – doped parent sample	0.92	0.91

Figure 34: Transport no. values of samples at T = 30 °C

All the samples displayed ionic transport number close to 1.0. This implies that all the electrolyte materials are good ionic conductor with negligible electronic conductivity. Thus they are promising electrolyte candidates for solid-state sodium ion batteries.

## 5 Conclusion

- In  $\text{Na}_3\text{V}_2(\text{PO}_4)_3$  (NVP) and  $\text{Na}_3\text{FeV}(\text{PO}_4)_3$  (NFP) samples, the expected phase was not formed.
- However, in  $\text{Na}_3\text{Fe}_2(\text{PO}_4)_3$  (NFP) the expected phase was successfully formed.
- $\text{Na}_3\text{Fe}_2(\text{PO}_4)_3$  (NFP) showed paramagnetic property at room temperature ( $T = 30^\circ \text{C}$ ) when measured using SQUID magnetometer.
- $\text{Na}_{3.3}\text{Zr}_{1.9}\text{Nb}_{0.1}\text{Si}_{2.4}\text{P}_{0.6}\text{O}_{12}$  (Nb-doped parent sample) showed higher ionic conductivity at room temperature (1.80 mS/cm).
- $\text{Na}_{3.2}\text{Zr}_2\text{Si}_{2.2}\text{P}_{0.8}\text{O}_{12}$  (parent sample),  $\text{Na}_{3.4}\text{Zr}_{1.9}\text{Zn}_{0.1}\text{Si}_{2.2}\text{P}_{0.8}\text{O}_{12}$  (Zn-doped parent sample),  $\text{Na}_{3.3}\text{Zr}_{1.9}\text{Nb}_{0.1}\text{Si}_{2.4}\text{P}_{0.6}\text{O}_{12}$  (Nb-doped parent sample) showed more than 90% ionic contribution to electrical conductivity at room temperature.



## 6 References

### References

- [1] L. Xiao X. Ai Y. Cao Y. Fang, J. Zhang and H. Yang. *Phosphate Framework Electrode Materials for Sodium Ion Batteries*, 4((1600392):1–21, 2017.
- [2] Clearfield A. Subramanian MA, Subramanian Rajeevi. Lithium ion conductors in the system  $\text{ab}_2(\text{po}_4)_3$ . *Solid State Ionics.*, 18-19:562–569, 1986.
- [3] Sadaoka Y Imanaka N Adachi G-y. Aono H, Sugimoto E. Ionic conductivity and sinterability of lithium titanium phosphate system. *Solid State Ionics.*, 40/41:38–42, 1990.
- [4] Kafalas JA. Goodenough JB, Hong HYP. Fast  $\text{Na}^+$ -ion transport in skeleton structures. *Mater Res Bull.*, 11(2):203-220, 1976.
- [5] Kierkegaard Peder. Hagman Lars Ove. The crystal structure of  $\text{Na}_2(\text{po}_4)_3$  (me=ge, ti, zr). *Acta Chemica Scand.*, 22:1822–1832, 1968.
- [6] Lü X et al. Zhou W, Xue L.  $\text{Na}_x\text{M}_y(\text{po}_4)_3$  (m = mn, fe, [ref.]ni) structure and properties for sodium extraction. *Nano Lett.*, 16(12):7836–7841, 2016.
- [7] Li H et al. Duan W, Zhu Z.  $\text{Na}_3\text{V}_2(\text{po}_4)_3@C$  core-shell nanocomposites for rechargeable sodium-ion batteries. *J Mater Chem A*, 2(23):789–1011, 2014.
- [8] R.A. Shakoor Y.Jung J.W. Choi S.Y.Lim, H.Kim. *J. Electrochem. Soc.*, 159(A):1393, 2012.
- [9] R. David O. Mentre M. Courty-C. Masquelier J. N. Chotard, G.Rousse. *Chem.Mater.*, 27:5982, 2015.
- [10] X. Ji Z.Jian, Y. Sun. *Chem. Commun*, 51:6381, 2015.
- [11] Cherkaoui F Brochu R Leflem G. Delmas C, Olazcuaga R. New family of phosphates with formula  $\text{Na}_3\text{M}_2(\text{po}_4)_3$  (m = ti, v, cr, fe). *Article. Comptes Rendus de l 'Academie Bulg des Sci*, 285(5):169–171, 1978.

- [12] Sigaryov SE Terziev VG. Lyubutin IS, Melnikov OK. Phase transitions in  $\text{Na}_3\text{Fe}_2(\text{PO}_4)_3$ : an inside view. *Solid State Ionics*, 31(3):197–201, 1988.
- [13] Usman M. Hou Y. Ahsan M.T., Ali Z. Unfolding the structural features of nasicon materials for sodium-ion full cells. *Carbon Energy*, 4:776–819, 2022.
- [14] Chroneos A. Kuganathan N. Defect chemistry and Na-ion diffusion in  $\text{Na}_3\text{Fe}_2(\text{PO}_4)_3$  cathode material. *Materials*, 12(8):1348, 2019.
- [15] Zhang J Xia Y Chen T-Zhang S Liu Y, Zhou Y. Monoclinic phase  $\text{Na}_3\text{Fe}_2(\text{PO}_4)_3$ : synthesis, structure, and electrochemical performance as cathode material in sodium-ion batteries. *ACS Sustainable Chem Eng.*, 5(2):1306–1314, 2016.
- [16] Couturier JC Quarton M. Tillement O, Angenault J. Electrochemical studies of mixed valence nasicon. *Solid State Ion*, 53-56:391–399, 1992.
- [17] D. Wang; X. Bie; Q. Fu; D. Dixon; N. Bramnik; Y.S. Hu; F. Fauth; Y. Wei; H. Ehrenberg; G. Chen; F. Du. Sodium vanadium titanium phosphate electrode for symmetric sodium-ion batteries with high power and long lifespan. *Nat Commun.*, 8:15888, 2017.
- [18] Fauth F et al. Bianchini M, Brisset N.  $\text{Na}_3\text{V}_2(\text{PO}_4)_2\text{F}_3$  revisited: a high-resolution diffraction study. *Chem Mater.*, 26(14):4238-4247, 2014.
- [19] R.A. Shakoor Y.Jung J.W. Choi S.Y.Lim, H.Kim. Phase transitions in the  $\text{Na}_3\text{M}_2(\text{PO}_4)_2\text{F}_3$  family ( $\text{M} = \text{Al}^{3+}, \text{V}^{3+}, \text{Cr}^{3+}, \text{Fe}^{3+}, \text{Ga}^{3+}$ ): synthesis, thermal, structural, and magnetic studies. *J Solid State Chem.*, 148(1):260–277, 1999.
- [20] Rousse G et al. Yan G, Mariyappan S. Higher energy and safer sodium ion batteries via an electrochemically made disordered  $\text{Na}_3\text{V}_2(\text{PO}_4)_2\text{F}_3$  material. *Nat Commun.*, 10:585, 2019.
- [21] Goñi A et al. Serras P, Palomares V. High voltage cathode materials for Na-ion batteries of general formula  $\text{Na}_3\text{V}_2\text{O}_{2x}(\text{PO}_4)_2\text{F}_{3-2x}$ . *J Mater Chem.*, 22(41):22301-22308., 2012.
- [22] Dimitrova OV. Massa W, Yakubovich OV. Crystal structure of a new sodium vanadyl(IV) fluorophosphate  $\text{Na}_3\text{V}_2\text{O}_2\text{F}[\text{PO}_4]_2$ . *Solid State Sci.*, 4(4):495-501, 2002.

- [23] Tarascon JM Baudrin E. Sauvage F, Quarez E. Crystal structure and electrochemical properties vs.  $\text{Na}^+$  of the sodium fluorophosphate  $\text{Na}_{1.5}\text{VPO}_4\text{F}_{0.5}$ . *Solid State Sci.*, 8(10):1215-1221, 2006.
- [24] Zhao J Hu Y-S Liu H Dai S. Qi Y, Mu L. Superior  $\text{Na}$ -storage performance of low-temperature-synthesized  $\text{Na}_3(\text{VOPO}_4)_2\text{F}_{1+2x}$  ( $0 \leq x \leq 1$ ) nanoparticles for  $\text{Na}$ -ion batteries. *Angew Chem Int Ed.*, 54(34):9911-9916, 2015.
- [25] Sun J et al. Yang Z, Li G. High performance cathode material based on  $\text{Na}_3\text{V}_2(\text{PO}_4)_2\text{F}_3$  and  $\text{Na}_3\text{V}_2(\text{PO}_4)_3$  for sodium-ion batteries. *Energy Storage Mater.*, 25:724-730, 2020.
- [26] Kim Y-i et al. Park JY, Shim Y. An iron-doped nasicon type sodium ion battery cathode for enhanced sodium storage performance and its full cell applications. *J Mater Chem A.*, 8(39):20436-20445, 2020.
- [27] Lee MH Kim H Lee S Kang K. Kim J, Yoon G. New 4v-class and zero-strain cathode material for  $\text{Na}$ -ion batteries. *Chem Mater.*, 29(18):7826-7832, 2017.
- [28] Seongsu Lee Hyunchul Kim Kyu-Young Park Young-Uk Park Haegyeom Kim Jongsoon Kim Hee-Dae Lim Won-Sub Yoon Hyungsub Kim, Inchul Park and Kisuk Kang. Rhombohedral nasicon-type  $\text{Na}_x\text{Fe}_2(\text{SO}_4)_3$  for sodium ion batteries: comparison with phosphate and alluaudite phases. *Chemistry of Materials*, 25(18):3614–3622, 2013.
- [29] Xiao J et al. Chen M, Hua W. Nasicon-type air-stable and all-climate cathode for sodium-ion batteries with low cost and high-power density. *Nat Commun.*, 10:1480, 2019.
- [30] Lee S et al. Kim H, Park I. Understanding the electro- chemical mechanism of the new iron-based mixed-phosphate  $\text{Na}_4\text{Fe}_3(\text{PO}_4)_2(\text{P}_2\text{O}_7)$  in a  $\text{Na}$  rechargeable battery. *Chem Mater.*, 25(18):3614-3622, 2013.
- [31] Yuan T et al. Pu X, Wang H.  $\text{Na}_4\text{Fe}_3(\text{PO}_4)_2(\text{P}_2\text{O}_7)/\text{C}$  nano- spheres as low-cost, high-performance cathode material for sodium-ion batteries. *Energy Storage Mater.*, 22:330-336, 2019.

- [32] Wang S et al. Zhang L-m, He X-d. Hollow-sphere-structured  $\text{Na}_4\text{Fe}_3(\text{PO}_4)_2(\text{P}_2\text{O}_7)/\text{C}$  as a cathode material for sodium-ion batteries. *ACS Appl Mater Interfaces.*, 13(22):25972-25980, 2021.
- [33] Zhou W Goodenough JB. Shiva K, Singh P.  $\text{NaFe}_2\text{PO}_4(\text{SO}_4)_2$ : a potential cathode for a Na-ion battery. *Energy Environ Sci.*, 9(10):3103-3106, 2016.
- [34] Lander L Lu J Yamada A. Chung S-C, Ming J. Rhombohedral NASICON-type  $\text{Na}_x\text{Fe}_2(\text{SO}_4)_3$  for sodium ion batteries: comparison with phosphate and alluaudite phases. *J Mater Chem A.*, 6(9):3919-3925, 2018.
- [35] Mahmoud A et al. Essehli R, Alkhateeb A. Optimization of the compositions of polyanionic sodium-ion battery cathode  $\text{NaFe}_2\text{Vx}(\text{PO}_4)(\text{SO}_4)_2$ . *J Power Sources.*, 469(A):228417, 2020.
- [36] Hamdi Ben Yahia, Rachid Essehli, Ruhul Amin, Khalid Boulahya, Toyoki Okumura, and I. Belharouak. Sodium intercalation in the phosphosulfate cathode  $\text{NaFe}_2(\text{PO}_4)(\text{SO}_4)_2$ . *Journal of Power Sources*, 382:144–151, 04 2018.
- [37] Arroyo y de Dompablo ME Vezin H Tarascon JM Palacín MR. Senguttuvan P, Rousse G. Low-potential sodium insertion in a NASICON-type structure through the  $\text{Ti(III)/Ti(II)}$  redox couple. *J Am Chem Soc.*, 135(10):3897-3903, 2013.
- [38] Okada S Yamaki J-i. Park SI, Gocheva I. Electrochemical properties of  $\text{NaTi}_2(\text{PO}_4)_3$  anode for rechargeable aqueous sodium-ion batteries. *J. Electrochem. Soc.*, 158(10):A1067-A1070, 2011.
- [39] Hong HYP. Crystal structures and crystal chemistry in the system  $\text{Na}_1+\text{xZr}_2\text{SixP}_3\text{O}_{12}$ . *Mater Res Bull.*, 11(2):173-182, 1976.
- [40] Kolli SK et al. Deng Z, Sai Gautam G. Phase behavior in rhombohedral NASICON electrolytes and electrodes. *Chem Mater.*, 32(18):7908-7920, 2020.
- [41] Wang A et al. Zou Z, Ma N. relationships between  $\text{Na}^+$  distribution, concerted migration, and diffusion properties in rhombohedral NASICON. *Adv Energy Mater.*, 10(30):2001486, 2020.